UHASSELT
KNOWLEDGE IN ACTION

Maastricht University

Faculty of Medicine and Life Sciences
School for Life Sciences
Master of Biomedical Sciences

Master's thesis

Characterization of DUX4 in A549 and SW982 cells and its Role in Arthritis

Dario Cosemans

Thesis presented in fulfillment of the requirements for the degree of Master of Biomedical Sciences, specialization Molecular Mechanisms in Health and Disease

SUPERVISOR :

Prof. dr. Pieter RUYTINX

MENTOR :

Mevrouw Elien LUYTEN

2023
2024

Transnational University Limburg is a unique collaboration of two universities in two countries: the University of Hasselt and Maastricht University.

UHASSELT
KNOWLEDGE IN ACTION

www.uhasselt.be
Universiteit Hasselt
Campus Hasselt:
Martelarenlaan 42 | 3500 Hasselt
Campus Diepenbeek:
Agoralaan Gebouw D | 3590 Diepenbeek

Maastricht University

Faculty of Medicine and Life Sciences
School for Life Sciences
Master of Biomedical Sciences

Master's thesis

Characterization of DUX4 in A549 and SW982 cells and its Role in Arthritis

Dario Cosemans

Thesis presented in fulfillment of the requirements for the degree of Master of Biomedical Sciences, specialization Molecular Mechanisms in Health and Disease

SUPERVISOR :

Prof. dr. Pieter RUYTINX

MENTOR :

Mevrouw Elien LUYTEN

Characterization of DUX4 in A549 and SW982 cells and Its Role in Arthritis

Dario Cosemans[1], Elien Luyten[1,2], and Prof. dr. Pieter Ruytinx[1,2]

[1]Faculty of Medicine and Life Sciences, Hasselt University, Campus Diepenbeek, Agoralaan Building D - 3590 Diepenbeek – Belgium
[2]Immunology & Infection research group, Biomedical Research Institute, Hasselt University, Campus Diepenbeek, Agoralaan Gebouw C - 3590 Diepenbeek, Belgium

Running title: *The role of DUX4 in arthritis (< 50 characters inc. spaces, italic)*

To whom correspondence should be addressed: Pieter Ruytinx, Tel: +32 (11) 26 93 45; Email: pieter.ruytinx@uhasselt.be

Keywords: Inflammatory arthritis, DUX4, fibroblast-like synoviocytes (FLS), transfection, overexpression

ABSTRACT

Double-homeobox protein 4 (DUX4) is a transcription factor in early embryogenesis and is epigenetically silenced in somatic tissues. In previous research, the presence of DUX4 auto-antibodies (UH-axSpA-IgG.8) in the plasma of axial spondyloarthritis patients and DUX4 re-expression in the synovium of arthritis patients was observed (1). To investigate the role of DUX4 in arthritis, the synovial sarcoma SW982 cell line will be characterized. Additionally, DUX4 overexpression will be optimized in A549 cells.

***DUX4* mRNA expression was investigated using nested PCR. DUX4 target gene expression, antioxidant, and apoptotic markers were assessed using qPCR. Next, patient-derived DUX4 antibodies were affinity-purified and used in immunocytochemistry. To study DUX4 overexpression, A549 lung carcinoma cells were defined and transfected with the pCIneo-DUX4 vector using FuGENE® HD or Lipofectamine™3000.**

Nested PCR indicates that DUX4 mRNA is present in A549 and SW982 cells, yet low baseline levels of target gene mRNA were detected. Immunofluorescent staining of A549 and SW982 with purified UH-axSpA-IgG.8 antibodies showed a cytoplasmic staining pattern. A549 cells were transfected successfully using FuGENE®HD, underscored by DUX4 detection using regular PCR and a clear presence of DUX4 target genes. No clear induction of antioxidant or apoptotic markers was observed upon transfection

INTRODUCTION

In 2020, our research group used a complementary DNA (cDNA) phage-display library expressing antigens from hip synovial tissue of three axial spondyloarthritis (axSpA) patients to screen plasma samples for novel antibody biomarkers. Here, antibodies against UH (Hasselt University)-axSpA-IgG.8, corresponding to the C-terminal part of double homeobox 4 (DUX4), were identified in the plasma of early axSpA patients (1). Additionally, DUX4 protein was discovered in synovial tissue of axSpA and RA patients but not healthy controls (1). More precisely, immunohistochemical staining of synovial tissue showed cells resembling cells reminiscent of fibroblast-like synoviocytes to re-express DUX4 in axSpA and RA patients but not in healthy controls (1). These findings suggest a potential function of DUX4 in arthritis, but its role remains to be elucidated.

Double homeobox 4 (DUX4) is a transcription factor transiently expressed during early embryogenesis (2). As maternal proteins and RNAs gradually degrade after fertilization, zygotic genome activation (ZGA) occurs (3). DUX4 expression gradually increases and peaks at the 4-cell stage but is epigenetically silenced after the 8-cell stage in most somatic tissues, excluding the thymus and testis, where it has unknown functions (2, 4). In mice, a *DUX4* orthologue, *Duxbl*, is specifically expressed just before T-cell receptor β-chain selection (5, 6). This selection is crucial in T cell development, and failed rearrangement of the β-chain will induce apoptosis (5-9). Therefore, human DUX4 may play a similar role in the human thymus. Furthermore, *DUX4* mRNA transcripts and protein have also been described in testes, specifically near the periphery of the seminiferous tubuli in cells with spermatocyte characteristics and spermatogonia (10). Like the processes in the thymus, apoptosis is a crucial step in spermatogenesis, characterized by high cell turnover (11). Moreover, DUX4 expression is also described in the differentiation of mesenchymal stem cells into osteoblast, bone-forming cells through upregulation of p21 (12). p21 induces cell cycle arrest, blocking proliferation while enabling complete differentiation (13). This demonstrates that DUX4 has normal physiological functions in addition to its role in early embryogenesis.

DUX4 in pathology

Aberrant DUX4 re-expression is associated with several pathologies, such as facioscapulohumeral muscular dystrophy (FSHD) and cancer (14-16). However, the biological effects of dysregulated DUX4 expression differ greatly between pathologies.

FSHD is an autosomal dominant type of muscle dystrophy in which the epigenetic silencing of *DUX4* is disrupted (17). The *DUX4* gene is encoded within the D4Z4 microsatellite repeat region located in the subtelomeric region of chromosome 4 (4q35). In healthy individuals, this region comprises 11 – 100 repeats. Each repeat consists of *DUX4* exon 1, including the coding sequence (CDS), intron 1, and exon 2 (**Figure 1A**) (18). Epigenetic silencing of the D4Z4 repeat involves DNA hypermethylation and histone modifications such as deacetylation and methylation, promoting heterochromatin formation and transcriptional inaccessibility. However, aberrant epigenetic activation by hypomethylation and chromatin remodeling may lead to the development of FSHD (**Figure 1B**). In 95% of patients, this activation is achieved through contraction of the D4Z4 repeats to 1 – 10 repeats (FSHD1, OMIM 158900) (17, 19). The remaining 5% of patients lack these contractions but carry mutations in epigenetic modifier proteins such as Structural Maintenance Of Chromosomes Flexible Hinge Domain Containing 1 (SMCHD1) or DNA-methyltransferase 3 beta (DNMT3B) that are involved in histone modification and DNA methylation, respectively (FSHD2, OMIM 158901) (**Figure 1B**) (19-22).

Nonetheless, DUX4 re-expression is only achievable in the presence of a permissive 4qA haplotype in which the last D4Z4 repeat is immediately followed by a pLAM region containing exon 3, which includes the non-canonical polyadenylation signal (pAs), ATTAAA (16). mRNA transcripts that use this pAs are stabilized and translated into functional protein. In contrast, the 4qB haplotype is non-permissive due to the absence of the pLAM region. Interestingly, a highly homologous D4Z4 repeat region is present at chromosome 10 (10q26, D10Z10), which has the distal pLAM region but lacks the canonical pAs (ATCAAA instead of ATTAAA) (16, 23). In somatic tissues, the 10q26 repeat region is non-

permissive and does not render polyadenylated DUX4 transcripts (**Figure 1C**) (16). Surprisingly, Snider *et al*. showed that *DUX4* polyadenylated mRNA transcripts in the testis are derived from both chromosomes 4 and 10. Intriguingly, chromosome 10 transcripts use an alternative pAs in exon 7, while chromosome 4 transcripts prefer the pAs in exon 3 over exon 7 (10).

Different *DUX4* mRNA splice variants were described, which are denoted as *DUX4* full-length (*DUX4*-fl) and *DUX4* short (*DUX4*-s) (**Figure 1C**) (10, 24). *DUX4*-s mRNA uses a cryptic splice site in the *DUX4* open-reading frame (ORF), leading to a truncated protein (10, 24). This truncated protein contains the DNA-binding homeodomains but lacks the transcriptional activation domain (TAD) that normally enables the transcriptional factor function of DUX4. The *DUX4*-fl mRNA has two subvariants, one retaining intron 1 and the other having intron 1 spliced out. Both transcripts render the same functional protein (**Figure 1A** and **C**) (24). *DUX4*-fl mRNA is not expressed in somatic tissue, but *DUX4*-s is. *DUX4*-s is shown to be expressed in control fibroblast. When these cells were converted into induced pluripotent stem cells (iPSCs), *DUX4*-s disappeared, but *DUX4*-fl was expressed. Differentiation to embryoid bodies reverted the change in expression pattern. In FSHD, *DUX4*-fl was expressed in fibroblasts, iPSCs, and embryoid bodies derived from these fibroblasts (10).

As a transcription factor, DUX4 is present in the nucleus and induces the expression of target genes. Through target genes, such as Paired-like Homeodomain 1 (*PITX1)*, Zinc Finger and Scan Domain Containing 4 (*ZSCAN4)*, Tripartite Motif Family 43 (*TRIM43)*, Methyl-CpG Binding Domain Protein 3 Like 2 (*MBD3L2)*, and PRAME Family Member 1 (*PRAMEF1)*, DUX4 re-activates a ZGA program (25). Through this program, DUX4 is associated with toxic pathways that inhibit cycle progression (13), oxidative stress, and DNA damage, inhibiting muscle cell differentiation and apoptosis (26).

In **cancer**, the re-expression of DUX4 can play either a pro- or antitumoral role, depending on the specific type of cancer. DUX4 expression activates an embryonic program in solid tumors, enabling MHC type I downregulation (15). This prevents the presentation of tumor-associated antigens on the cell surface and impairs cytotoxic T-cell function. Additionally, DUX4 re-expression is correlated with lower transcript levels of T-cell recruiting chemokines such as CXCL9 and CXCL10, enabling immune evasion and tumor survival (27).

In contrast, in colorectal cancer, DUX4 has been identified as a direct inhibitor of cyclin-dependent kinase 1 (CDK1), an important cell cycle regulator (14). Activation of NFκB by tumor necrosis factor alpha (TNF-α) induces the expression of NF-E2-related factor 3 (NFE2L3), a negative regulator of *DUX4*. Inhibition of NFκB and an NFE2L3 knockdown has shown an increase in DUX4 expression and a decrease in cell growth and proliferation, indicating DUX4 as a tumor suppressor in colorectal cancer (14). Interestingly, NFE2L3 knockdown successfully upregulated endogenous DUX4 in HCT116 and HT27 cells but, unlike in FSHD, did not induce any changes in apoptosis, while overexpression of exogenous DUX4 did in colon cancer cells (14). While DUX4 was described primarily in FSHD, more evidence suggests an additional role of DUX4 in normal physiology and pathophysiology, such as cancer, arrhinia, and potentially arthritis (1, 14, 28).

Arthritis

Arthritis is a heterogeneous group of systemic joint diseases characterized by acute or chronic inflammation of the joints, often presented with tenderness, swelling, pain, and stiffness of the affected joint, leading to joint damage and joint deformation when left untreated (29). Over 100 different types of arthritis are described, making diagnosis challenging. *Rheumatoid arthritis (RA)* and *spondyloarthritis (SpA)* are the two most frequent systemic forms of chronic auto-immune inflammatory arthritis, affecting 1,0 and 2,0 % of individuals worldwide, respectively (30, 31). RA mainly affects the smaller joints of the hands and feet but can involve any synovial joint. The onset of RA is gradual, with often a polyarthritic and symmetrical pattern (32). In SpA, sacroiliac and spinal joints are affected, leading to low back pain that worsens by night but improves with exercise.

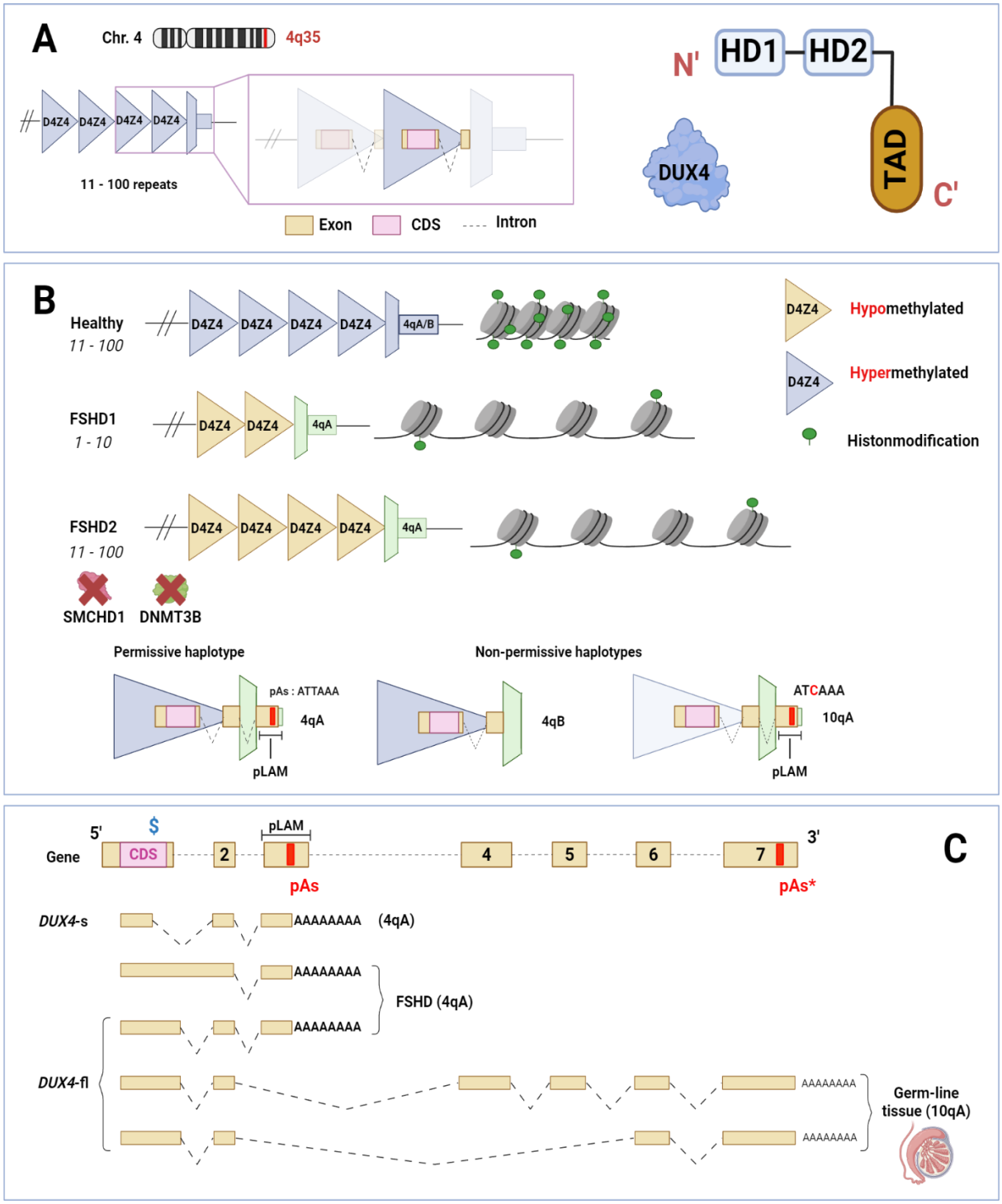

Figure 1 - Overview of DUX4 on chromosomal, gene, and protein levels. A) D4Z4 macrosatellite repeat region on a chromosomal and chromatin level. **B)** DUX4 re-expression in facioscapulohumeral dystrophy (FSHD). **C)** DUX4 mRNA transcript variants as visualized by Snider et al. (10). The blue $ indicates a cryptic splice site in exon 1. *Chr 4, chromosome 4; CDS, coding sequence; DUX4, Double homeobox protein 4; HD1 and 2, homeodomain 1 and 2; TAD, transactivation domain; N', N-terminus; C', C-terminus; SMCHD1, Structural Maintenance Of Chromosomes Flexible Hinge Domain Containing 1; DNMT3B, DNA-methyl transferase 3 beta; DUX4-s, DUX4-short; DUX4-fl, DUX4-full-length; pAs, polyadenylation site; FSHD, facioscapulohumeral dystrophy.*

While RA and SpA have different clinical pictures, both are characterized by synovitis, inflammation of the synovial membrane that lines the inside of the joint capsule. In RA, joint inflammation leads to bone loss (33), while in SpA, bone is formed ectopically (34). Unlike inflammatory arthritis, in osteoarthritis (OA), biomechanical stress on the cartilage results in

cartilage degeneration and remodeling of the subchondral bone (35). Although inflammation is not considered the driving force of OA, OA patients show features of secondary synovial inflammation (36).

In *healthy joints*, the synovium consists of a thin inner lining layer of macrophages and fibroblast-like synoviocytes (FLS) with a collagen-rich sublining layer containing blood vessels, nerve supply, and fat cells (37). However, T-cells, B-cells, plasma cells, macrophages, and FLS are present in low numbers in the sublining (37). FLS produce extracellular matrix (ECM) components such as hyaluronic acid, lubricin, and collagens but also controlled levels of ECM degrading enzymes such as matrix metalloproteinases (MMPs) to control ECM turnover, nourish cartilage, and provide structural integrity and lubrication to the joint (38-40). Anti-inflammatory cytokines, such as IL-1 receptor antagonist are more abundantly present than inflammatory cytokines, such as tumor necrosis factor-alpha (TNF-α) and interleukin-1 (IL-1β), thus establishing an anti-inflammatory environment (37). Furthermore, bone remodeling is tightly regulated by close communication between bone-forming osteoblasts and bone-resorbing osteoclasts to maintain a net unchanged amount of bone (41). When an excess of bone is present, osteoblasts produce more receptor activator of NF kappa B ligand (RANKL) (41). RANKL induces osteoclast formation by binding to its receptor RANK on osteoclast-precursor cells. Osteoclasts resorb the excess bone and release growth factors that attract osteoblasts to the site. These osteoblasts produce osteoprotegerin (OPG) that blocks excessive bone resorption by inhibiting RANKL (42-44). FLS can produce both RANKL and OPG, but under physiological conditions, a slightly higher amount of OPG is present in FLS (37).

During *joint inflammation*, the synovium changes notably due to hyperplasia of the synovial lining layer, the accumulation of recruited immune cells, and increasing numbers of activated FLS. In *RA*, an aggressive pannus consisting of mainly hyperplastic FLS, infiltrated macrophages, and T cells produce high levels of pro-inflammatory cytokines such as TNF-α, IL-1β, and IL-6 (45). These cytokines enable FLS to produce more RANKL while downregulating the production of OPG, promoting the formation of osteoclasts that resorb subchondral bone (46). Furthermore, inflamed FLS produce chemokines such as CCL20, CCL2, and CXCL8, promoting immune cell influx (47, 48). TNF-α triggers these newly recruited immune cells to produce additional RANKL and FLS to produce Dickkopf 1 (DDK-1), which inhibits osteoblast formation (49). Macrophages produce IL-23 that shift T-cells towards a T_H17 phenotype. These T_H17 cells produce IL-17, which directly promotes osteoclastogenesis by binding to osteoclast-progenitor cells and indirectly through activation of FLS, thereby inhibiting osteoblast differentiation. Additionally, FLS express increased levels of MMPs such as MMP1 and MMP3 that can break down cartilage (39). This cartilage breakdown by MMPs enables further pannus infiltration and articular erosion, leading to irreversible joint destruction. In SpA, FLS also acquire a hyperplastic phenotype, leading to articular erosion. Furthermore, FLS can differentiate into osteoblast-precursor cells that contribute to ectopic bone formation at bone and entheses, places where ligaments and tendons connect to bone. Besides articular inflammation, SpA is also characterized by inflammation of entheses. The exact cause of ectopic bone formation is not yet fully understood. However, evidence suggests that ectopic bone formation is influenced by the intrinsic transcriptional signature of these FLS (50). Moreover, FLS in SpA produce IL-26 which induces bone mineralization in osteoblasts (51).

Diagnosis of RA is made using a combination of clinical symptoms, imaging, and the presence of biomarkers such as anti-citrullinated protein (ACPA) and rheumatic factor (RF). In SpA, HLA-B27 is a risk factor for developing SpA. To date, treatment of arthritis aims to limit pain and improve joint functionality. For RA and SpA, disease-modifying anti-rheumatic drugs (DMARDs), like methotrexate (MTX), are the first-line prescribed medication. MTX influences FLS by decreasing the production of MMPs, pro-inflammatory cytokines, and RANKL, impeding bone resorption (52-54).

EXPERIMENTAL PROCEDURES

Cell culture A549, SW982 and HeLa cells

Cells are cultured in growth medium (DMEM, ref 41966-029, Gibco, United Kingdom) with 10% fetal bovine serum (FBS) (ref. S00FL10D01, biowest, France) and 1% penicillin-streptomycin (P/S) (ref. 15140-122, Gibco, United States) at 10,000 (A549 and HeLa) and 7000 cells/cm² (SW982) density and maintained at 37°C and 5% CO_2.

RNA isolation

According to the manufacturer's instructions, total RNA was isolated from cells using the RNeasy® Mini Kit (Qiagen, The Netherlands). Two DNase treatments, on-column and in-liquid, were included to remove genomic DNA. Following the in-liquid treatment, samples were cleaned, using the RNA cleanup protocol, to remove residual DNase I. RNA concentration was measured using NanoDrop™2000 (Thermo Scientific, United States).

cDNA synthesis

After RNA isolation, mRNA was converted into cDNA using qScript (ref. 84035, Quantabio, United States). First, 1000 ng RNA was diluted in nuclease-free water, heated for 5' at 65°C, and immediately placed on ice to break GC bonds. Next, qScript was added to an end volume of 20 µL, and samples were loaded in a thermocycler using the following program: 5' at 22°C, 30' at 42°C, 5' at 85°C, and ∞ at 4°C, lid temperature 95°C.

Nested PCR

Due to the low abundance of DUX4 mRNA, nested PCR was used. Here, two PCRs are executed in sequence to increase sensitivity and specificity. Each PCR reaction contained the following components in a 20 µL reaction volume: nuclease-free water (Qiagen), 1X PCR buffer (Roche, Switzerland, 11 435 094 001), 10 pmol forward/reverse primer (Supplementary Table S1), 1X dNTPs (ref. 03 622613 001, Roche, Switzerland) and 1 U Taq polymerase (ref. 11435094001 Roche). Ultimately, 100 ng cDNA was used as input. The following thermocycler (T100, Biorad, United States) protocol was used: 5' at 95°C, followed by 15 cycles of 20" at 95°C, 40" at 58°C, and 1' at 72°C. the PCR reaction was ended with 5' at 72°C and ∞ at 4°C, lid temperature 105°C. After the first PCR, the product was cleaned with 1,5 µL of Exo-ZAP (ref. 7200100-1000, Amplicon, Denmark) using the following protocol: 15' at 37°C, 15' at 80°C, and ∞ at 4°C, lid temperature 90°C. Lastly, 2 µL of cleaned PCR1 product was used in PCR2 consisting of 40 cycles.

Agarose gel electrophoresis and clean-up

The PCR product was visualized using agarose gel electrophoresis. A 2% agarose gel (Invitrogen, United States) was prepared using 1X TAE buffer and 1:10000 GelRed (Biotium, ref. 41003-1, United States. Bands of interest were excised and prepared for Sanger sequencing (Macrogen, The Netherlands) using the NucleoSpin® Gel and PCR clean-up kit (Macherey-Nagel, United Kingdom) according to manufacturer's instructions

Quantitative PCR

A quantitative PCR (qPCR) was performed to investigate gene expression using the QuantStudio3 (Applied Biosystems, United States) fast or standard protocol with the volume set at 10 µL (Supplementary Figure S3). For one reaction, the following reagents were used for a 10 µL reaction volume: 50 ng of cDNA (25 ng/µL), nuclease-free water (Qiagen), 1X Fast SYBR green master mix (ref. 4385612, Applied Biosystems), and 2,5 pmol forward/reverse primer (Supplementary Table S1).

Immunofluorescent staining

Approximately 26,000 cells/cm² were grown on glass coverslips for 24 h in a 24-well plate (Cellstar, Greiner, Austria) and washed three times with PBS (ref. 392-0433, VWR, United States). Next, the cells were fixated with cold acetone (-20°C) at 4°C for 10' and evaporated for 30'. After washing the wells three times with 1X PBS on a shaker, the 12-well plate was placed in a humidified chamber, and coverslips were submerged in 100% Dako protein block (ref. X0909, Dako, Denmark) for 30' at RT. Furthermore, the protein block was removed and diluted primary antibodies (Supplementary Table S2) were added and incubated overnight at 4°C. The next day, the coverslips were washed three times, and the secondary antibody, diluted in the respective host serum, was pipetted on the coverslips (Supplementary Table S2).

After a 1h incubation in the dark at RT, the coverslips were again washed three times, and the nuclei were stained using 1:10000 4', 6-diamino-2-phenylindole (DAPI) (ref. 62248, Thermo Scientific) for 10' at RT. Autofluorescence was blocked using 0,03% Sudan Black (ref. S2380-25G , Sigma, United States) in 70% EtOH for 10' at RT. Lastly, coverslips were mounted on glass slides using mounting medium (Fluoromount G, ref. 004958-02, Invitrogen), and slides were visualized using fluorescence microscopy (Leica, DM4000 B LED, Germany).

Regular 35-cycle PCR amplification for pCIneo-DUX4 vector characterization

Before investigating DUX4 overexpression in A549 cells, the pCIneo-*DUX4* vector (55) was characterized using a regular PCR analogous to the second PCR reaction of the nested PCR. However, for primer combinations that render a theoretical amplicon larger than 709 bp, a PCR ratio with a 1- or 3-minute elongation time was performed.

Transfection optimization of A549 cells with pCIneo-DUX4 vector

FuGENE® HD

A549 cells were seeded in a 12-well plate (cat. no. 665180, Cellstar, Greiner, Austria) at 20,000 cells/cm² density in growth medium for 24 h at 37°C and 5% CO_2. The following conditions were included *in duplo*: untransfected control, mock-transfected control (only FuGENE), non-transfected control (only plasmid DNA), 4:1 FuGENE/vector ratio, 2:1 ratio, and 1,5:1 ratio. Plasmid DNA was diluted to 1 µg/µL using nuclease-free water (Qiagen).

The next day, plasmid DNA and FuGENE®HD Transfection Reagent (ref. E2313, Promega, United States) in the appropriate ratios were combined in a serum-free medium (DMEM, Gibco) and incubated for 10' at RT. The culture medium was changed with a growth medium without P/S (Gibco). Lastly, the reaction mixture was added to the respective wells and incubated for 24 h and 48 h.

Lipofectamine™3000

A549 cells were seeded in a 12-well plate (Greiner) at 20,000 cells/cm² density in a growth medium for 24 h at 37°C and 5% CO_2. The following conditions were included *in duplo*: untransfected control, mock-transfected control (only lipofectamine), non-transfected control (only plasmid DNA), 3,8:1,8 lipofectamine/vector ratio, 2,8:1,8 ratio, and 1,8:1,8 ratio.

First, Lipofectamine™3000 Transfection Reagent (ref. 100022049, Invitrogen) was diluted in DMEM (Gibco) in the appropriate ratios. Next, plasmid DNA was mixed with P300 reagent (ref. 100022056, Invitrogen) in DMEM (Gibco). The latter dilutions were mixed with the respective diluted transfection reagent. Mixtures were incubated for 10-15' at RT. The culture medium was changed to a growth medium without P/S (Gibco). To conclude, incubated mixture was added to the cells and incubated at 37°C, 5% CO_2 for 24 h and 72 h.

Statistical analyses

Outliers were determined using the ROUT test (Q = 10 %) in GraphPad Prism 10. Equal variances were verified with the Brown-Forsythe test. To assess the normal distribution of the data the Shapiro-Wilk test was used. For data not normally distributed, non-parametric testing was done using a Kruskal-Wallis test, and post-hoc multiple comparison testing by Dunn's test comparing each group to the untransfected control group (Untr) was performed at a significance level of $\alpha = 0,05$. To assess differences in gene expression at different time points, a Mann-Whitney-U test was used with multiple comparisons relative to a control group using the Holm-Šidák method at a significance level $\alpha = 0,05$. All data was visualized with standard error mean (SEM).

RESULTS

Nested PCR to characterize DUX4 gene expression in A549 cells and SW982 cells

To investigate DUX4 gene expression in various cell lines and to distinguish different mRNA splice variants a nested PCR was used. A549 and SW982 cells were both positive for *DUX4* mRNA in which exon 3 was present. These cell lines show an amplicon at 200 bp and between 300 and 400 bp, respectively (**Figure 2** – Lane 2). Furthermore, A549 cells were positive for *DUX4* mRNA with exon 7 present as well, while SW982 cells were negative (**Figure 2** – Lane 3). HeLa cells were included as a negative control, already established by the research group (data not shown). The NTC and negative control were clean for exons 3 and 7, with only primer dimers at the bottom of the lanes (**Figure 2** – Lane 3 and 4).

A549 cells have a low baseline expression level of DUX4 targets compared to HeLa cells, while SW982 cells express higher levels of MBD3L2 and TRIM43.

Next, baseline DUX4 target gene expression was assessed with qPCR. A549 and SW982 cells showed a decreased expression of *ZSCAN4* and *PRAMEF1* than HeLa cells. Remarkably, SW982 cells tend to have a higher baseline expression of *MBD3L2* and *TRIM43* compared to HeLa and A549 cells (**Figure 3**).

DUX4 protein is present in the cytoplasmic of A549 and SW982 cells but not in the nucleus

To assess the presence of DUX4 protein in A549 and SW982 cells, immunofluorescent staining was performed using anti-human DUX4 antibodies purified using affinity chromatography (**Supplementary methods**). Vimentin staining was used to evaluate a successful staining procedure. Both A549 and SW982 cells showed cytoplasmic vimentin staining (**Figure 4A**, **B**, **G,** and **H**). Interestingly, staining with purified antibodies against UH-axSpA-IgG.8 (corresponding to the C-terminal part of DUX4) showed a cytoplasmic staining pattern. Moreover, a bright perinuclear region was visible. Surprisingly, the staining was limited to the cytoplasm and not visible in the nucleus (**Figure 4A** and **G**). All negative controls only showed nuclear DAPI staining (**Figure 4C**, **F**, **I,** and **L**).

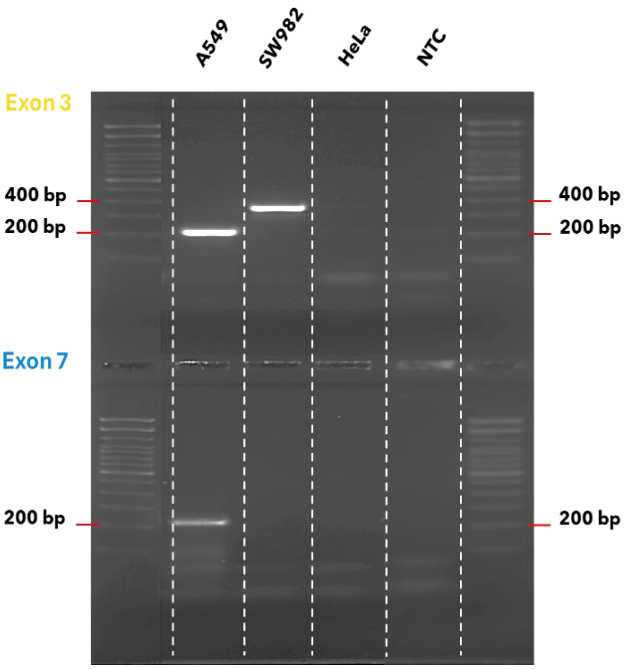

Figure 2 – A549 cells and SW982 cells are positive for DUX4 mRNA. PCR products were separated on a 2% agarose gel with a 100 bp DNA ladder. Upper part: exon 3 – A549 and SW982 cells were both positive for DUX4 transcripts containing exon 3. The NTC and HeLa were negative for *DUX4*, with no bands present in these lanes except primer dimers at the bottom. Lower part: exon 7 – Only A549 cells were positive for DUX4 transcripts containing exon 7. The NTC and HeLa were negative for *DUX4* with no bands present in these lanes except primer dimers at the bottom. Image was made using the D-DiGit® Gel Scanner at 8X exposure rate. *HeLa, Henrietta Lacks; NTC, no template control; bp, base pair.*

The insert of the pCIneo-DUX4 vector comprises exons 1-3 and introns 1-2

To investigate DUX4 overexpression in A549 cells, the pCIneo-*DUX4* vector (55) was used. A regular PCR was used to verify the integrity of the insert after bacterial amplification. Overlapping sequences were obtained by combining multiple primer sets (**Figure 5** – Top). While some amplicons ended up at the estimated height on the gel, most of them ended up either too low or too high (**Figure 5**). However, after excision of the bands and sequencing, they highly corresponded to the expected sequence (data not shown). Cross-referring the sequencing outputs in BLAST and alignment in Benchling indicate that exon 1, intron 1, exon 2, and exon 3 are fully present in the insert. Intron 2 was only partly present in some sequencing products. However, additional sequencing products showed the whole intron 2.

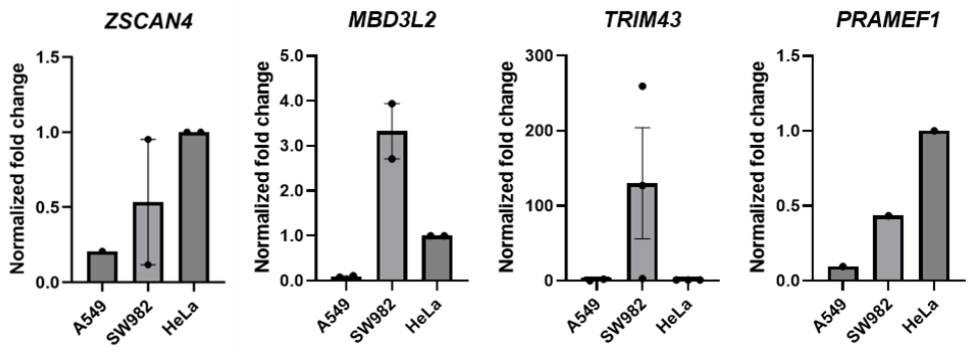

Figure 3 - A549 and SW982 express low baseline levels of DUX4 target genes using qPCR analysis. The $2^{(-\Delta\Delta Ct)}$ methods was used to calculate fold changes. Fold changes were normalized and compared to HeLa. A549 cells seem to express lower baseline levels of DUX4 target gene mRNA. SW982 cells seem to express lower levels of *ZSCAN4* and *PRAMEF1* mRNA but remarkably higher amounts of *MBD3L2* and *TRIM43* mRNA. *n = 1 to 3 for ZSCAN4, MBD3L2 and TRIM43. n = 1 for PRAMEF1. Error bars are shown as standard error mean (SEM). ZSCAN4, Zinc Finger and Scan Domain Containing 4; MBD3L2, Methyl-CpG Binding Domain protein 3 Like 2; TRIM43; Tripartite Motif Family 43; PRAMEF1, PRAME Family Member 1*

After 24 h and 48 h of transfection with FuGENE®HD, DUX4 mRNA levels were detectable with PCR with significant increases in target gene expression

Following the pCIneo-*DUX4* vector characterization, A549 cells were transfected to overexpress DUX4. Successful transfection was assessed via DUX4 target gene expression. In this study, we optimized two transfection protocols using different transfection reagents, FuGENE®HD (Promega) and Lipofectamine™3000 (Thermo Scientific). Upon transfection using FuGENE in a 4 to 1 ratio (4|1) of FuGENE®HD reagent to plasmid, DUX4 mRNA became detectable with a regular 35-cycle PCR (**Figure 6A**). This result is further supported by the significant increase in target gene expression in the 4|1 condition (**Figure 6B**). Target gene expression was increased in the 2|1 and 1,5|1 conditions. However, this increase was not statistically significant. In the three control groups of untransfected (Untr), mock-transfected (FuGENE), and non-transfected (DNA) cells, no *DUX4* band was visible after PCR amplification supported by baseline levels of DUX4 target genes (**Figure 3** and **Figure 6B**). No significant differences in DUX4 target gene expression were observed when comparing 24 h to 48 h incubation after transfection (Supplementary Figure S4).

CASP3 and BCL2 were significantly increased after transfection 24 h with FuGENE, while other stress genes were unaffected after 24 h or 48 h transfection

To assess the effects of DUX4 overexpression on cell death and apoptosis, we selected a panel of two antioxidant-related genes, Superoxide dismutase 1 (*SOD1)* and Glutathione peroxidase 1 (*GPX1*), and three apoptosis genes, BCL2 associated X apoptosis regulator (*BAX)*, B-cell lymphoma 2 (*BCL2)*, and Caspase-3 (*CASP3*). Following transfection with FuGENE®HD for 24 h and 48 h, *SOD1*, *GPX1*, and *BAX* levels did not significantly differ from the mRNA in the untransfected (Untr), mock transfected (FuGENE) or non-transfected (DNA) conditions. However, *CASP3* levels did increase after 24 h upon a 4:1 ratio transfection but decreased again after 48 h post-transfection, while the significant increase in *CASP3* remained in the non-transfected condition. Furthermore, *BCL2* mRNA ex-pression increased only after 24 h. Remarkably, the increase in *BCL2* and *CASP3* was also shown in the non-transfected condition (DNA). No statistically significant differences were observed comparing 24 h to 48 h (Supplementary Figure S4).

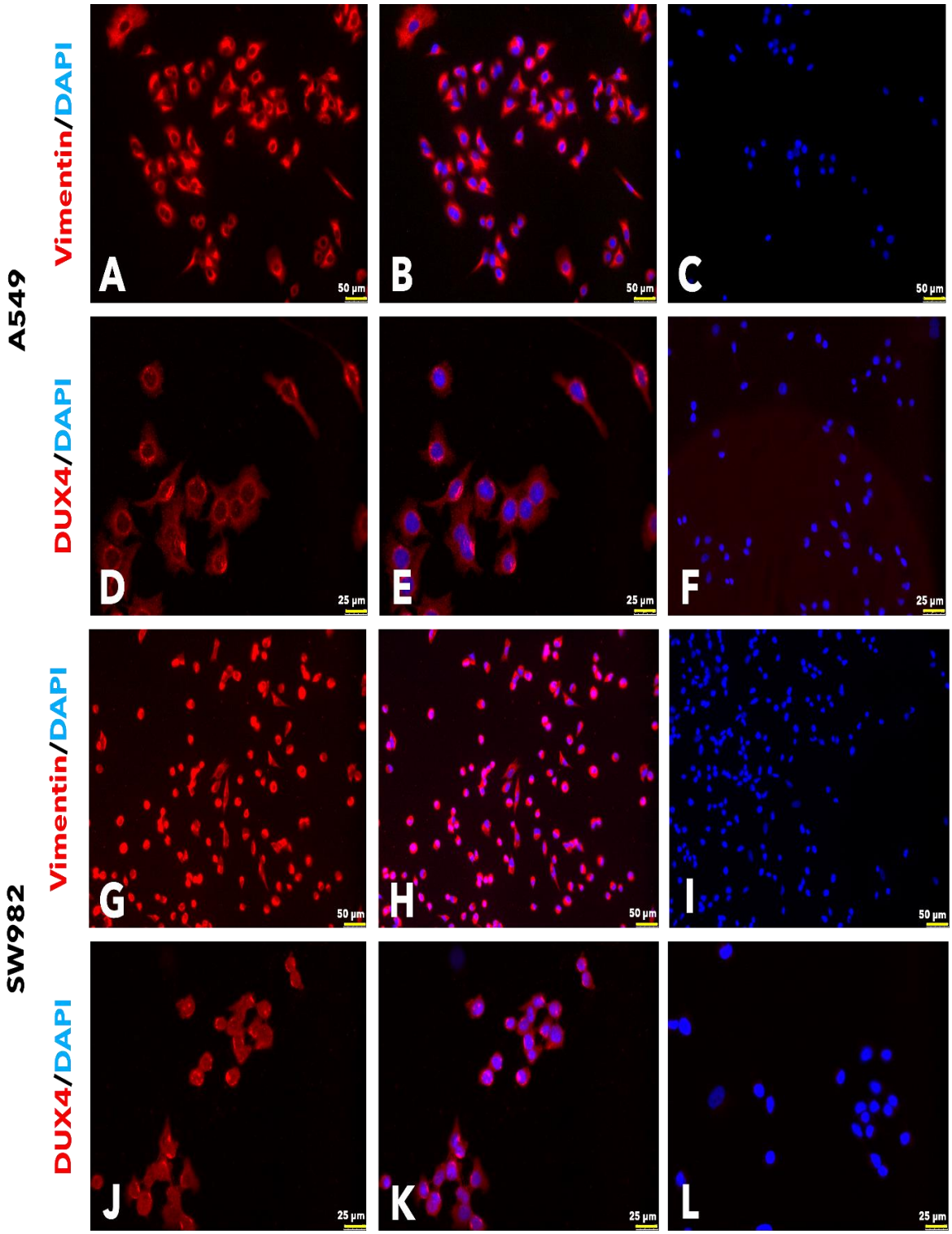

Figure 4 - A549 cells and SW982 both show a similar cytoplasmic DUX4 staining pattern. Vimentin staining using primary anti-mouse vimentin antibodies (1:200) and Alexa-Fluor-555 secondary goat-anti-mouse antibodies (1:500) (red). **A and B**) A549 cells were positive for vimentin and show a cytoplasmic staining pattern. **C)** Negative control for vimentin staining showing only nuclear DAPI staining (blue). A similar pattern was shown in SW982 cells (**G – I**). A549 cells (**D – E**) and SW982 cells (**J – K**) showed a similar cytoplasmic staining pattern for DUX4. Purified UH-axSpA-IgG.8 antibodies were diluted 1:4 for A549 cells and 1:3 for SW982 cells. Goat-anti-human antibodies labeled with Alexa-Fluor-555 were used as secondary antibody. Interestingly, the cytoplasmic staining is homogeneous distributed but with brighter perinuclear regions. Both negative controls showed only nuclear DAPI staining (F and L). Image A – C and G – I were taken at 20X magnification (scale bar: 50 µm). Image D – E and J – L were taken at 40X magnification (scale bar: 25 µm). *DUX4, Double-homeobox protein 4; DAPI, 4', 6-diamino-2-phenylindole; µm, micrometer.*

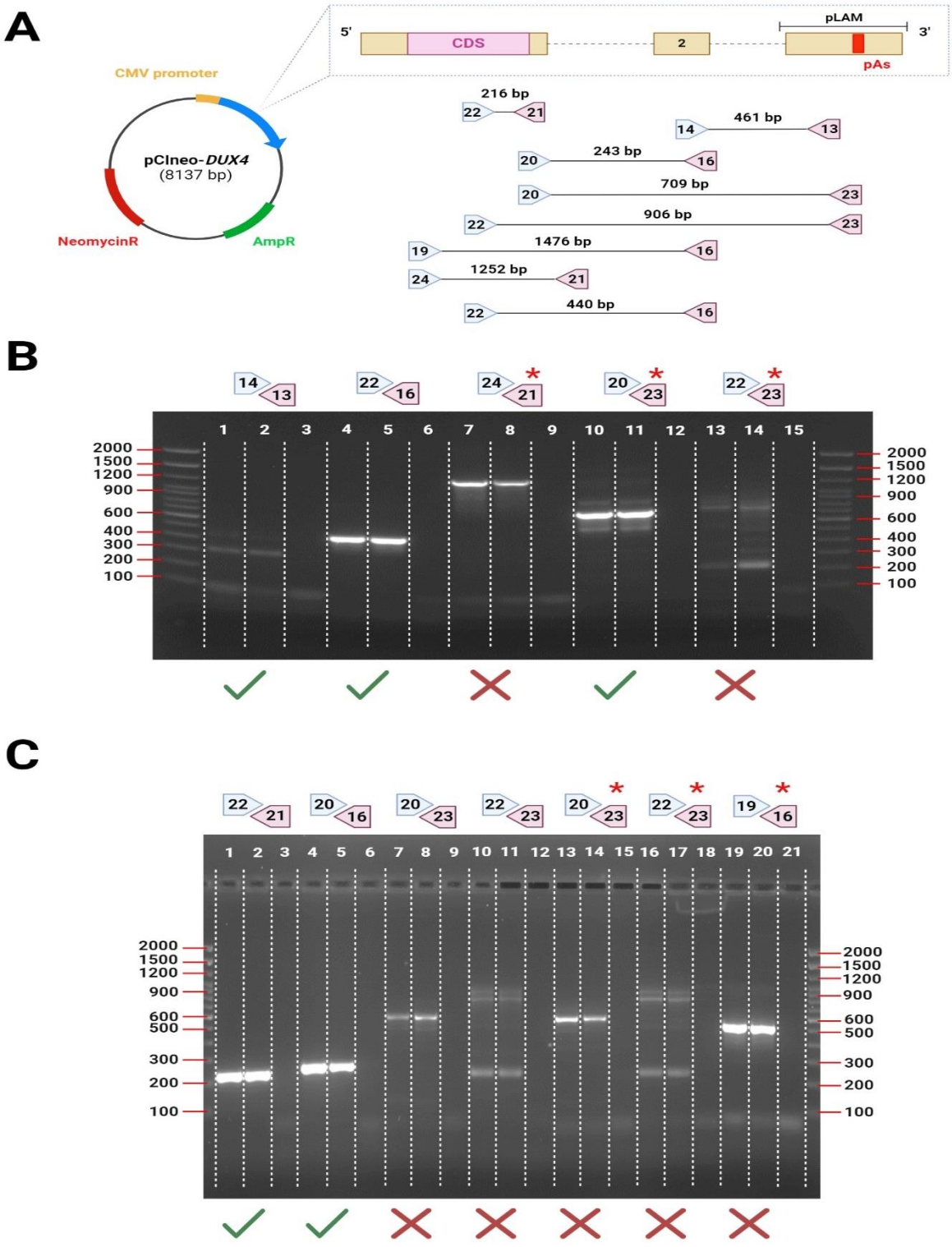

Figure 5 - The pCIneo-*DUX4* vector consists of exons 1 - 3 and the full introns 1 and 2. A) Overview of the theoretical insert according to Vanderplanck *et al. (55)* with the assessed primer combinations and the theoretical lengths. Below, representative 2% agarose gels are displayed. On the top gel (**B**), the first, second, and fourth primer combination gave the expected amplicon length (green check mark) while the third and fifth combination gave an amplicon lower than the theoretical size (red cross). On the bottom gel (**C**), the first two primer combination gave the expected amplicon lengths. However, for the remaining primer combinations the observed amplicon length did not correspond to the theoretical lengths. Gel images were taken using the D-DiGit Gel Scanner at 8X exposure rate. *CMV, cytomegalovirus; AmpR, ampiciline resistance gene; NeomycineR, neomycine resistance gene; bp, base pair; CDS, coding sequence; pAs, polyadenylation site, DUX4, Double-homeobox 4.*

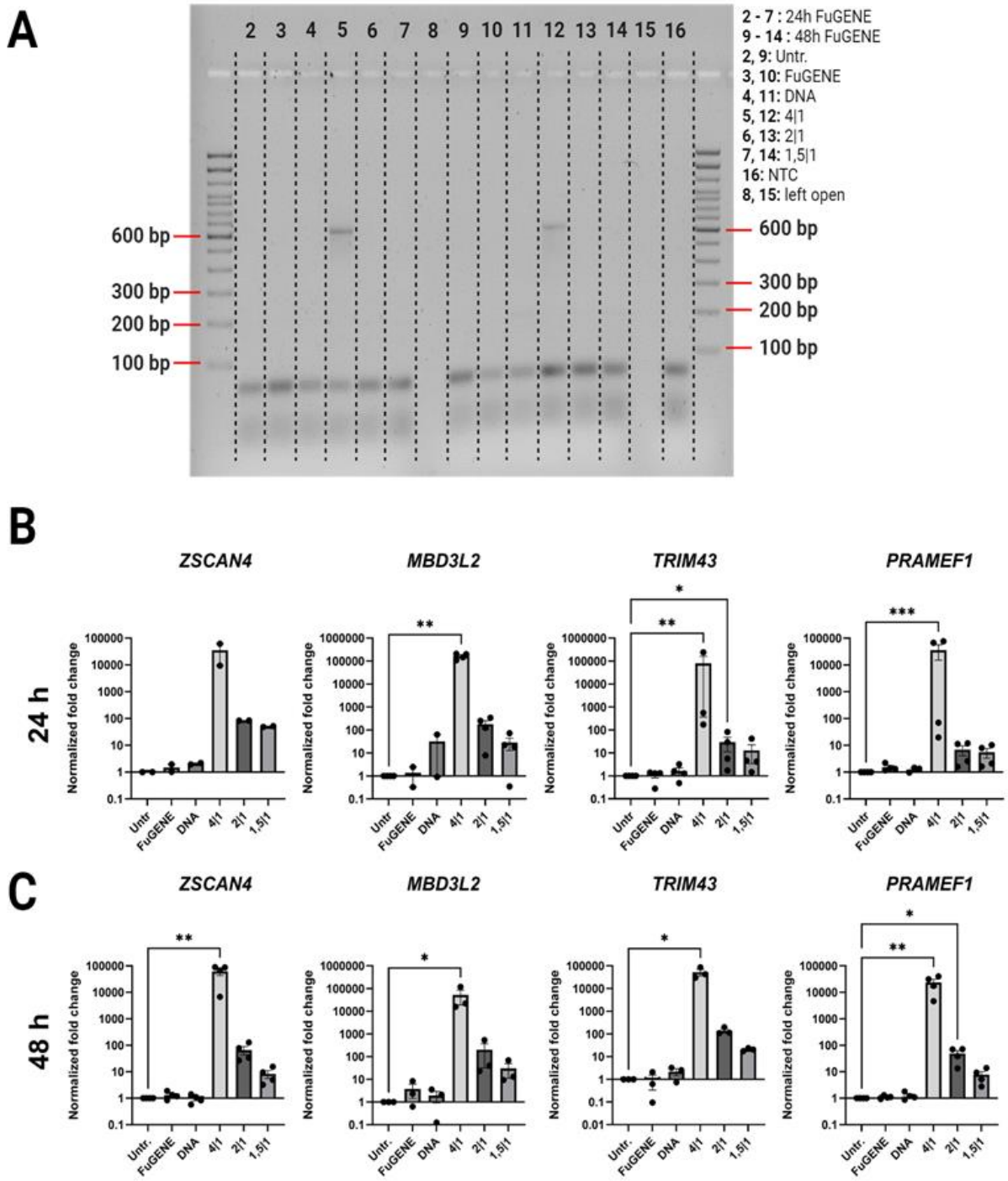

Figure 6 – DUX4 and target gene expression were significantly increased upon 24h and 48h transfection with FuGENE. The top panel **A** shows a representative regular 35-cycle PCR for each tested condition. The control groups, untransfected (Untr), mock transfected (FuGENE), and non-transfected (DNA), showed no detectable *DUX4* bands around 650 bp. However, at the 4|1 ratio an amplicon was present at 650 bp, corresponding to the expected amplicon size. The bottom panels **B** and **C** shows DUX4 target gene expression for the tested conditions at 24 h and 48 h. Fold changes were calculated using the $2^{-\Delta\Delta Ct}$ method and normalized to the untransfected control. A significant increase in target genes expression was detected after transfection in a 4|1 ratio of FuGENE:plasmid. Furthermore, an increase in DUX4 target gene expression was observed in the other transfected conditions. However, these were not statistically significant. The FuGENE and DNA condition showed comparable DUX4 target gene expression as the untransfected control. *Statistical significance was assessed using a Kruskal-Wallis test with post-hoc Dunn's multiple comparison test comparing each condition to the untransfected control, n = 2 – 4. Error bars are shown as standard error mean (SEM). * p < 0,05, ** p < 0,01, *** p < 0,001. bp, base pair; NTC, no template control; ZSCAN4, Zinc Finger and Scan Domain Containing 4; MBD3L2, Methyl-CpG Binding Domain protein 3 Like 2; TRIM43; Tripartite Motif Family 43; PRAMEF1, PRAME Family Member 1.*

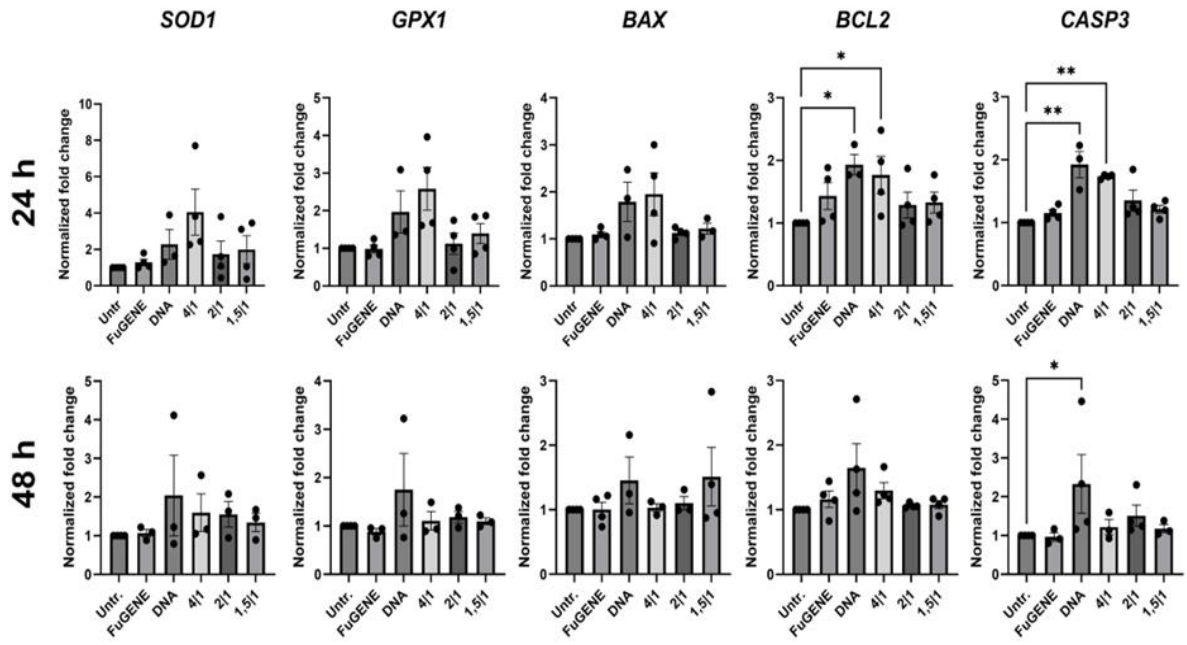

Figure 7 – *CASP3* and *BCL2* gene expression levels significantly increased upon 24 h transfection with FuGENE®HD in a 4|1 ratio. Fold changes were calculated using the $2^{-\Delta\Delta Ct}$ method and normalized to the untransfected control (Untr). After 24 h and 48 h transfection with FuGENE, no statistically significant changes in stress gene expression were observed for the three control groups (Unt, FuGENE, and DNA). For *SOD1*, *GPX1*, and *BAX*, transfection did not change gene expression notably. However, *BCL2* and *CASP3* expression were markedly increased after 24 h transfection in a 4:1 transfection ratio. After 48 h, *BCL2* showed gene expression levels similar to the control groups, but *CASP3* increased significantly in the non-transfected condition. Remarkably, the increase in *BCL2* and *CASP3* was also shown in the non-transfected condition (DNA). *n = 3 – 4, error bars are shown as SEM, . * p < 0,05, ** p < 0,01. SOD1, Superoxide dismutase; GPX1, glutathione peroxidase 1; BAX, BCL2 associated X apoptosis regulator, BCL2, B-cell lymphoma 2; CASP3, Caspase 3.*

Transfection with Lipofectamine™3000 for 72 h did not increase DUX4 mRNA above the PCR detection threshold but significantly increased DUX4 target gene expression

After 72 h transfection with Lipofectamine™3000, *DUX4* was over-expressed and significantly increased the expression of DUX4 target genes to a similar level in all conditions transfected with Lipofectamine™3000 in a different ratio to vector: 1,8:1,8 (Lipo 1,8), 2,8:1,8 (Lipo 2,8) and 3,8:1,8 (Lipo 3,8). However, no *DUX4* mRNA was detected using PCR. All three control groups (Untr, Mock, and DNA) showed no band on the agarose gel, which was confirmed by baseline levels of DUX4 target genes (Supplementary Figure S5 and S6).

CASP3 was significantly increased after 72 h transfection with Lipofectamine™3000 in a 3,8:1,8 ratio

Like transfection with Lipofectamine™3000, *SOD1*, *GPX1*, *BAX*, and *BCL2* levels were stable upon *DUX4* overexpression. A549 cells transfected with Lipofectamine™3000 in a 1,8 to 1,8 ratio Lipofectamine™3000 : plasmid (Lipo 1,8) or in a 2,8 to 1,8 ratio (Lipo 2,8) showed similar gene expression as the untransfected and mock-transfected control groups. However, *CASP3* mRNA levels were significantly increased in A549 cells transfected with Lipofectamine™3000 in a 3,8 to 1,8 ratio (Lipo 3,8) and the non-transfected control condition (DNA). (Supplementary Figure S7).

DISCUSSION

In this study, our goal was to characterize DUX4 in A549 and SW982 cells on both the mRNA and protein level. A549 cells are lung tumor cells and were shown to be positive for DUX4 mRNA in the past (data not shown). SW982 are synovial sarcoma cells are an accepted alternative cell line to study fibroblast-like synoviocytes (FLS) in the context of arthritis (56). Before performing functional tests, characterization of both cell types is preferable to understand their endogenous expression of DUX4-related genes and behavior during functional tests such as stimulation assays, silencing, or overexpression experiments.

We used **nested PCR** to study endogenous DUX4 expression in A549, SW982, and HeLa cells. Due to the low abundance of *DUX4* mRNA, a highly sensitive and specific nested PCR is necessary for its detection. The sensitivity and specificity were increased by using two consecutive PCRs using a first outer primer pair (Supplementary Figure **S1**) and a second inner primer pair (Supplementary Figure **S1**) in which the first amplicon is used as the template for the second PCR (10, 57). HeLa cells were negative for *DUX4* mRNA, as previously established by our research group (data not shown) (**Figure 2**). The Human Protein Atlas verified this absence of DUX4 mRNA in HeLa cells, as no *DUX4* mRNA transcripts per million (TPM) were detected in RNA sequencing experiments. The fragment size of the amplicons detected in A549 cells was around 200 and 250 bp and could correspond to *DUX4*-fl variants described by Snider *et al.* (10). Similar bands were sequenced in the past by our research group and did show high sequence alignment with the 211 bp transcript and 241 bp transcript, respectively (data not shown). According to RNA sequencing experiments, the Human Protein Atlas reinforces these results with 1,3 *DUX4* transcripts per million (TPM) present in A549 cells. The chromosomal origin of these A549 *DUX4* transcripts was also investigated through sequencing (data not shown). Chromosome 10 specific SNPs were identified in exon 2 (data not shown), as previously by Snider *et al.* (10). The amplicon height of the SW982 DUX4 transcript corresponds to 347 bp, a *DUX4*-fl transcript previously identified by Snider *et al.* (10). These data are in contrast to the findings in the Human Protein Atlas, showing no *DUX4* transcripts in SW982 cells. However, since A549 and SW982 cells are tumor cells, these may also acquire a germ-line character by which we would expect both transcripts like previously described by Snider et al. (10). However, in SW982 cells, only the exon 3 transcript seems to be expressed, which may indicate that *DUX4* transcripts are transcribed from chromosome 4 instead of chromosome 10, like in A549 cells (10). However, the chromosomal origin of this transcript in SW982 cells has not yet been investigated and deserves future attention.

Next, we aimed to investigate DUX4 protein expression in the indicated cell lines. Therefore, axSpA-IgG.8 antibodies towards the C-terminal end of the DUX4 protein were purified from a patient with axSpA using affinity chromatography (**Supplementary methods**) Next, these antibodies were used to **immunofluorescently stain DUX4** in A549 and SW982 cells, and we reported exclusively a cytoplasmic staining and none in the nucleus (**Figure 4**). If DUX4 is absent in the nucleus, it cannot function as a transcription factor. Both cell types' low target gene expression further supported these findings (**Figure 3**). Yet, for SW982 cells, *MBD3L2* and *TRIM43* were clearly expressed at higher levels than in HeLa cells (**Figure 3**). However, the discussed DUX4 targets are not exclusively induced by DUX4; other upstream regulators, such as NF-κB, could also regulate their expression (58). In contrast, in FSHD, DUX4 was exclusively stained in the nucleus and associated with high target gene expression levels in FSHD myotubes (59).

Interestingly, the Human Protein Atlas shows, using immunocytochemistry, that the DUX4 protein is present in the nucleus, as is expected of a functional transcription factor. Yet, there are some differences between our staining and the one from the Human Protein Atlas. Firstly, we used purified human antibodies towards the C-terminal end of DUX4. In the Human Protein Atlas Project, a rabbit-anti-DUX4 antibody (Sigma, HPA058451) towards an epitope located in the N-terminal part of DUX4 was used. Similar proteins can share epitopes, leading to cross-reactivity in immune assays. This could lead to misleading data on protein identification, expression levels, and location. Besides DUX4, homologs, such as DUX4c, are described that share the N-terminal part of DUX4 but not the C-terminal end. Therefore, the

nuclear staining observed in the Human Protein Atlas could be due to DUX4c reactivity or a combination of DUX4 and DUX4c. By using purified antibodies towards the C-terminal part of DUX4, we circumvented this homolog problem and showed no nuclear staining. Secondly, different fixation methods were used which can influence the epitope availability. In this study, we used an acetone fixation, while the Human Protein Atlas used a para-formaldehyde (PFA) fixation. PFA fixation preserves the localization of cellular components and proteins by making crosslinks. However, a downside of PFA is the potential epitope masking, which makes the antibody binding inefficient. Acetone fixation dehydrates and permeabilizes the cells and can induce denaturation and precipitation of proteins, which could also lead to epitope masking. Therefore, it could be that the acetone fixation in our staining did cause damage to the nuclear membrane, leading to leakage of nuclear proteins, such as DUX4, to the cytoplasm (60, 61).

In the past, our research repeated the staining as performed before by the Human Protein Atlas using PFA. Additionally, the same staining was also executed with acetone fixation. The staining with PFA fixation did show cytoplasmic and nuclear staining, while acetone fixation showed only a cytoplasmic staining pattern (data not shown). In the future, the staining with purified UH-axSpA-IgG.8 antibodies should be repeated using PFA fixation to verify the results seen by the Human Protein Atlas or to verify our results. PFA could be advantageous because of the better preservation of the location of cellular components.

Besides the fixation method, detection using fluorescently labeled secondary antibodies could give a distorted view of the actual location of the protein. Interestingly, the cytoplasmic staining looks homogeneous throughout the cytoplasm, with bright perinuclear regions. Antibodies are reasonably large compared to the nucleus. Therefore, the observed location and the actual location of the protein differ. By this, it could be that the protein has started to leak out of the nucleus due to acetone-induced membrane damage. Yet, some DUX4 could still be present inside the nucleus but falsely localized to the cytoplasm because of resolution issues. Confocal microscopy could solve this issue by offering a better resolution. As a negative control, the same staining could also be performed on HeLa cells.

To study the effect of DUX4 overexpression in A549 cells, these cells were transfected with the pCIneo-*DUX4* vector (Promega). Vanderplanck *et al.* previously characterized the insert, indicating it consists of exons 1 – 3 and both introns 1 and 2 (55). We set up a **vector characterization** experiment using multiple primer combinations to verify these findings. The primer sets were used to provide overlapping amplicons and maximize coverage. After amplification using a regular 35-cycle PCR, amplicons were visualized using agarose gel electrophoresis. Some amplicons did end up at the theoretical band height, and the subsequent Sanger sequencing (Macrogen) and alignment in BLAST and Benchling verified this. However, the observed band height did not meet our expectations for amplicons with a theoretical length of 461 bp and higher. Moreover, multiple bands were observed for some primer combinations. These amplicons were excised from the gel and sequenced. Surprisingly, alignment showed that these amplicons, although not being present at the expected height, did correspond to a part of the expected amplicon. A possible cause for multiple bands is cleavage by exo or endonucleases or excessive shear forces after amplification. Moreover, aspecific binding of primers, primer dimers, or hairpin structure formation could lead to the formation of shorter amplicons. However, no primer dimers were detected on the gel electrophoresis (**Figure 5**) Overall, the longer amplicons did end up lower than expected on the gel. This could be due to irregular migration speed leading to an uneven migration of the amplicons through the gel. Ultimately, we confirm the characterization of Vanderplanck *et al*. (55). Exon 1 and 2 and intron 1 and 2 are entirely present in the insert (**Figure 5**). However, with the applied primer combinations, we could only verify the presence of a part of exon 3. Based on the literature and these results, we could conclude that exon 3 is completely present in the insert. Yet, a future experiment could be conducted to verify the presence of the last part of exon 3, including the pAs. Ideally, a primer combination that renders a theoretical amplicon overlapping with the amplicon observed in our experiment should be used. This could be achieved using primer 14

and a T3-reverse primer that binds 3' of exon 3 in the vector backbone.

Transfection of A549 cells with FuGENE in a 4 to 1 ratio of FuGENE/vector increased *DUX4* gene expression to levels above the detection threshold of a general 35-cycle PCR, as opposed to the nested PCR detection method for endogenous DUX4. This result is supported by the significant increase in target gene expression at the 4:1 transfection ratio (**Figure 6**). The other two transfected conditions (2|1 and 1,5|1) showed moderately increased target gene expression despite no DUX4 mRNA detection by the 35-cycle PCR. Target gene expression decreased when cells were transfected with less FuGENE but the same amount of plasmid DNA. The absence of amplicon on the agarose gel after a regular PCR could be due to mRNA levels that were too low for a general PCR to detect in the 2:1 and 1,5:1 conditions. Moreover, 10 ng of cDNA was used in the PCR, which is low for a *DUX4* PCR, considering we have to use 100 ng cDNA for the nested PCR to detect endogenous *DUX4*. In the future, a nested PCR could be used to assess *DUX4* expression after transfection. Additionally, overexpression should also be verified directly on the protein level using a Western Blot or mass spectrometry. Upon 72 h transfection of A549 cells with Lipofectamine™3000, DUX4 target gene expression increased when compared to baseline but was not statistically significant (Supplementary Figure **S5**. However, no *DUX4* mRNA was detected with PCR. This can also be due to the relatively small amount of start material used, considering we used 100 ng of start material for the nested PCR. The transfected conditions (Lipo 1,8; Lipo 2,8 and Lipo 3,8) all showed similar levels of DUX4 target genes. Our results correspond to other DUX4 overexpression experiments using the same vector. DUX4 target genes increased upon transfection (55, 59, 62, 63).

In FSHD, DUX4 re-expression induces ROS damage and apoptosis in muscle cells (26, 64). Therefore, a decrease in *SOD1*, *GPX1*, and anti-apoptotic *BCL2* was expected. Furthermore, an increase in pro-apoptotic *BAX* and *CASP3* was anticipated. Interestingly, *SOD1*, *GPX1*, and *BAX* gene expression did not alter upon transfection (**Figure 6**). However, A549 lung tumor cells could exhibit inherent resistance to ROS damage. Tumor cells are known to regulate compensation mechanisms that prevent damage and apoptosis and promote survival. ROS production could be monitored using the Incucyte and ROS-specific dyes in future experiments.

Moreover, *BAX* and *BCL2* were expressed at comparable levels for most of the conditions. Normally, slightly more anti-apoptotic BCL2 is produced than the pro-apoptotic BAX to keep the cell from dying. In FSHD, a pro-apoptotic shift drives muscle cells toward apoptosis (65). Interestingly, a significant increase in *BCL2* gene expression was detected in the 4|1 ratio after 24 h or 48 h FuGENE transfection and after 72 h transfection with Lipofectamine™3000 in a 3,8 to 1,8 ratio, indicating the cells became anti-apoptotic. Yet, this increase was also observed in the non-transfected condition. This may imply the increase in BCL2 mRNA is caused by the addition of vector and not because of DUX4 overexpression. However, considering the spread of our data and the low sample size, more experiments are needed to verify this increase. Furthermore, an increase in mRNA does not translate to increased protein expression. Therefore, future protein expression should also be assessed using Western Blot. Remarkably, *CASP3* gene expression was increased notably as well in these conditions. However, the same observation was made in the non-transfected control indicating that the increase in CASP3 mRNA is likely an effect of the addition of vector and not due to DUX4 overexpression. CASP3 is the downstream effector in the apoptotic pathway and has to be cleaved to be active and induce apoptosis (66). Further studies on protein levels are needed. Like ROS production, CASP3 activation could be implemented in an Incucyte experiment using CASP3/7 dyes. Besides apoptosis, future studies should also focus on the effects on cell proliferation and survival using an Alamar Blue or MTT assay and Ki67 or BrdU-staining.

Overall, our results on DUX4 overexpression indicate successful transfection of A549 cells with a significant increase in DUX4 target gene expression. However, we did not quantify the transfection efficiency but can deduce from our results that the 4:1 ratio was the most efficient ratio for FuGENE®HD transfection. For Lipofectamine™3000, qPCR data shows that all transfection ratios likely had a similar efficiency. Therefore, quantifying

efficiency should first be addressed by transfecting cells with a pCIneo vector of comparable size with a fluorescent marker such as GFP. The pCIneo-*Fluc-EGFP* plasmid (Addgene, ref. 90170) could be used. Additionally, transfection with the empty vector backbone must be included to rule out any backbone-related effect and verify the observed effects are induced due to DUX4 overexpression. Lastly, overexpression experiments in SW982 cells will be performed after optimization. Thereby, the effect of DUX4 re-expression in arthritis could be investigated.

CONCLUSION

In this study, DUX4 expression was investigated in A549 and SW982 cells. Due to its low transcript abundance, a nested PCR strategy was used to detect *DUX4* mRNA levels, which report that A549 cells were positive for mRNA from chromosome 10 (data not shown) and that these transcripts could use the pAs in exon 3 or 7. SW982 cells were positive for *DUX4* mRNA that uses the exon 3 pAs. However, the chromosomal origin of the SW982 DUX4 transcripts is still unknown and could be addressed in future experiments. We observed a cytoplasmic staining pattern with patient-derived antibodies in which DUX4 protein is excluded from the nucleus in both A549 and SW982 cells. We successfully transfected A549 cells with FuGENE®HD in different ratios and were able to detect *DUX4* with a regular 35-cycle PCR using the highest amount of FuGENE®HD. Upon transfection of A549 cells, DUX4 target gene expression increased significantly, while genes involved in anti-oxidant mechanisms did not alter gene expression. Pro-apoptotic BAX remained stable, while anti-apoptotic *BCL2* and pro-apoptotic *CASP3* increased significantly on mRNA level. Further studies to verify these results on protein levels are needed.

REFERENCES

1. Quaden D, Vandormael P, Ruytinx P, Geusens P, Corten K, Vanhoof J, et al. Antibodies Against Three Novel Peptides in Early Axial Spondyloarthritis Patients From Two Independent Cohorts. Arthritis Rheumatol. 2020;72(12):2094-105.
2. Hendrickson PG, Dorais JA, Grow EJ, Whiddon JL, Lim JW, Wike CL, et al. Conserved roles of mouse DUX and human DUX4 in activating cleavage-stage genes and MERVL/HERVL retrotransposons. Nat Genet. 2017;49(6):925-34.
3. Dobson AT, Raja R, Abeyta MJ, Taylor T, Shen S, Haqq C, et al. The unique transcriptome through day 3 of human preimplantation development. Hum Mol Genet. 2004;13(14):1461-70.
4. De Iaco A, Planet E, Coluccio A, Verp S, Duc J, Trono D. DUX-family transcription factors regulate zygotic genome activation in placental mammals. Nat Genet. 2017;49(6):941-5.
5. Kawazu M, Yamamoto G, Yoshimi M, Yamamoto K, Asai T, Ichikawa M, et al. Expression profiling of immature thymocytes revealed a novel homeobox gene that regulates double-negative thymocyte development. J Immunol. 2007;179(8):5335-45.
6. Klein F, Mitrovic M, Roux J, Engdahl C, von Muenchow L, Alberti-Servera L, et al. The transcription factor Duxbl mediates elimination of pre-T cells that fail beta-selection. J Exp Med. 2019;216(3):638-55.
7. Mocciaro E, Runfola V, Ghezzi P, Pannese M, Gabellini D. DUX4 Role in Normal Physiology and in FSHD Muscular Dystrophy. Cells. 2021;10(12).
8. Falk I, Nerz G, Haidl I, Krotkova A, Eichmann K. Immature thymocytes that fail to express TCRbeta and/or TCRgamma delta proteins die by apoptotic cell death in the CD44(-)CD25(-) (DN4) subset. Eur J Immunol. 2001;31(11):3308-17.
9. Mallick CA, Dudley EC, Viney JL, Owen MJ, Hayday AC. Rearrangement and diversity of T cell receptor beta chain genes in thymocytes: a critical role for the beta chain in development. Cell. 1993;73(3):513-9.
10. Snider L, Geng LN, Lemmers RJ, Kyba M, Ware CB, Nelson AM, et al. Facioscapulohumeral dystrophy: incomplete suppression of a retrotransposed gene. PLoS Genet. 2010;6(10):e1001181.
11. Weinbauer GF, Aslam H, Krishnamurthy H, Brinkworth MH, Einspanier A, Hodges JK. Quantitative analysis of spermatogenesis and apoptosis in the common marmoset (Callithrix jacchus) reveals high rates of spermatogonial turnover and high spermatogenic efficiency. Biol Reprod. 2001;64(1):120-6.
12. de la Kethulle de Ryhove L, Ansseau E, Nachtegael C, Pieters K, Vanderplanck C, Geens M, et al. The Role of D4Z4-Encoded Proteins in the Osteogenic Differentiation of Mesenchymal Stromal Cells Isolated from Bone Marrow. Stem Cells Dev. 2015;24(22):2674-86.
13. Xu H, Wang Z, Jin S, Hao H, Zheng L, Zhou B, et al. Dux4 induces cell cycle arrest at G1 phase through upregulation of p21 expression. Biochem Biophys Res Commun. 2014;446(1):235-40.
14. Bury M, Le Calve B, Lessard F, Dal Maso T, Saliba J, Michiels C, et al. NFE2L3 Controls Colon Cancer Cell Growth through Regulation of DUX4, a CDK1 Inhibitor. Cell Rep. 2019;29(6):1469-81 e9.
15. Chew GL, Campbell AE, De Neef E, Sutliff NA, Shadle SC, Tapscott SJ, et al. DUX4 Suppresses MHC Class I to Promote Cancer Immune Evasion and Resistance to Checkpoint Blockade. Dev Cell. 2019;50(5):658-71 e7.
16. Lemmers RJ, van der Vliet PJ, Klooster R, Sacconi S, Camano P, Dauwerse JG, et al. A unifying genetic model for facioscapulohumeral muscular dystrophy. Science. 2010;329(5999):1650-3.
17. van Deutekom JC, Wijmenga C, van Tienhoven EA, Gruter AM, Hewitt JE, Padberg GW, et al. FSHD associated DNA rearrangements are due to deletions of integral copies of a 3.2 kb tandemly repeated unit. Hum Mol Genet. 1993;2(12):2037-42.
18. Ansseau E, Domire JS, Wallace LM, Eidahl JO, Guckes SM, Giesige CR, et al. Aberrant splicing in transgenes containing introns, exons, and V5 epitopes: lessons from developing an FSHD mouse model expressing a D4Z4 repeat with flanking genomic sequences. PLoS One. 2015;10(3):e0118813.
19. van Overveld PG, Lemmers RJ, Sandkuijl LA, Enthoven L, Winokur ST, Bakels F, et al. Hypomethylation of D4Z4 in 4q-linked and non-4q-linked facioscapulohumeral muscular dystrophy. Nat Genet. 2003;35(4):315-7.
20. Engal E, Sharma A, Tagatga N, Bentata M, Jaffe-Herman S, Geminder O, et al. SMCHD1 loss triggers DUX4 expression by disrupting splicing in FSHD2. bioRxiv. 2023.
21. Sacconi S, Lemmers RJ, Balog J, van der Vliet PJ, Lahaut P, van Nieuwenhuizen MP, et al. The FSHD2 gene

SMCHD1 is a modifier of disease severity in families affected by FSHD1. Am J Hum Genet. 2013;93(4):744-51.
22. van den Boogaard ML, Lemmers R, Balog J, Wohlgemuth M, Auranen M, Mitsuhashi S, et al. Mutations in DNMT3B Modify Epigenetic Repression of the D4Z4 Repeat and the Penetrance of Facioscapulohumeral Dystrophy. Am J Hum Genet. 2016;98(5):1020-9.
23. de Greef JC, Frants RR, van der Maarel SM. Epigenetic mechanisms of facioscapulohumeral muscular dystrophy. Mutat Res. 2008;647(1-2):94-102.
24. Snider L, Asawachaicharn A, Tyler AE, Geng LN, Petek LM, Maves L, et al. RNA transcripts, miRNA-sized fragments and proteins produced from D4Z4 units: new candidates for the pathophysiology of facioscapulohumeral dystrophy. Hum Mol Genet. 2009;18(13):2414-30.
25. Smith AA, Nip Y, Bennett SR, Hamm DC, Lemmers R, van der Vliet PJ, et al. DUX4 expression in cancer induces a metastable early embryonic totipotent program. Cell Rep. 2023;42(9):113114.
26. Bosnakovski D, Xu Z, Gang EJ, Galindo CL, Liu M, Simsek T, et al. An isogenetic myoblast expression screen identifies DUX4-mediated FSHD-associated molecular pathologies. EMBO J. 2008;27(20):2766-79.
27. Pineda JMB, Bradley RK. DUX4 is a common driver of immune evasion and immunotherapy failure in metastatic cancers. bioRxiv. 2023.
28. Inoue K, Bostan H, Browne MR, Bevis OF, Bortner CD, Moore SA, et al. DUX4 double whammy: The transcription factor that causes a rare muscular dystrophy also kills the precursors of the human nose. Sci Adv. 2023;9(7):eabq7744.
29. Smolen JS, Aletaha D, McInnes IB. Rheumatoid arthritis. Lancet. 2016;388(10055):2023-38.
30. Allado E, Moussu A, Bigna JJ, Hamroun S, Camier A, Chenuel B, et al. Global prevalence of spondyloarthritis in low-income and middle-income countries: a systematic review and meta-analysis protocol. BMJ Open. 2020;10(10):e041180.
31. Finckh A, Gilbert B, Hodkinson B, Bae SC, Thomas R, Deane KD, et al. Global epidemiology of rheumatoid arthritis. Nat Rev Rheumatol. 2022;18(10):591-602.
32. Smolen JS, Aletaha D, Barton A, Burmester GR, Emery P, Firestein GS, et al. Rheumatoid arthritis. Nat Rev Dis Primers. 2018;4:18001.
33. Kareem R, Botleroo RA, Bhandari R, Ogeyingbo OD, Ahmed R, Gyawali M, et al. The Impact of Rheumatoid Arthritis on Bone Loss: Links to Osteoporosis and Osteopenia. Cureus. 2021;13(8):e17519.
34. Nakamura A, Talukdar A, Nakamura S, Pathan E, Haroon N. Bone formation in axial spondyloarthritis: Is disease modification possible? Best Pract Res Clin Rheumatol. 2019;33(6):101491.
35. Guilak F. Biomechanical factors in osteoarthritis. Best Pract Res Clin Rheumatol. 2011;25(6):815-23.
36. Sokolove J, Lepus CM. Role of inflammation in the pathogenesis of osteoarthritis: latest findings and interpretations. Ther Adv Musculoskelet Dis. 2013;5(2):77-94.
37. Smith MD. The normal synovium. Open Rheumatol J. 2011;5:100-6.
38. Jay GD, Britt DE, Cha CJ. Lubricin is a product of megakaryocyte stimulating factor gene expression by human synovial fibroblasts. J Rheumatol. 2000;27(3):594-600.
39. Sabeh F, Fox D, Weiss SJ. Membrane-type I matrix metalloproteinase-dependent regulation of rheumatoid arthritis synoviocyte function. J Immunol. 2010;184(11):6396-406.
40. Schumacher BL, Block JA, Schmid TM, Aydelotte MB, Kuettner KE. A novel proteoglycan synthesized and secreted by chondrocytes of the superficial zone of articular cartilage. Arch Biochem Biophys. 1994;311(1):144-52.
41. Clarke B. Normal bone anatomy and physiology. Clin J Am Soc Nephrol. 2008;3 Suppl 3(Suppl 3):S131-9.
42. Anderson DM, Maraskovsky E, Billingsley WL, Dougall WC, Tometsko ME, Roux ER, et al. A homologue of the TNF receptor and its ligand enhance T-cell growth and dendritic-cell function. Nature. 1997;390(6656):175-9.
43. Boyce BF, Xing L. The RANKL/RANK/OPG pathway. Curr Osteoporos Rep. 2007;5(3):98-104.
44. Simonet WS, Lacey DL, Dunstan CR, Kelley M, Chang MS, Luthy R, et al. Osteoprotegerin: a novel secreted protein involved in the regulation of bone density. Cell. 1997;89(2):309-19.
45. Estell EG, Murphy LA, Gangi LR, Shah RP, Ateshian GA, Hung CT. Attachment of cartilage wear particles to the synovium negatively impacts friction properties. J Biomech. 2021;127:110668.
46. Hashizume M, Hayakawa N, Mihara M. IL-6 trans-signalling directly induces RANKL on fibroblast-like synovial cells and is involved in RANKL induction by TNF-alpha and IL-17. Rheumatology (Oxford). 2008;47(11):1635-40.
47. Alaaeddine N, Hilal G, Baddoura R, Antoniou J, Di Battista JA. CCL20 stimulates proinflammatory mediator synthesis in human fibroblast-like synoviocytes through a MAP kinase-dependent process with transcriptional and posttranscriptional control. J Rheumatol. 2011;38(9):1858-65.
48. Cagnard N, Letourneur F, Essabbani A, Devauchelle V, Mistou S, Rapinat A, et al. Interleukin-32, CCL2, PF4F1 and GFD10 are the only cytokine/chemokine genes differentially expressed by in vitro cultured rheumatoid and osteoarthritis fibroblast-like synoviocytes. Eur Cytokine Netw. 2005;16(4):289-92.
49. Diarra D, Stolina M, Polzer K, Zwerina J, Ominsky MS, Dwyer D, et al. Dickkopf-1 is a master regulator of joint remodeling. Nat Med. 2007;13(2):156-63.
50. Osta B, Roux JP, Lavocat F, Pierre M, Ndongo-Thiam N, Boivin G, et al. Differential Effects of IL-17A and TNF-alpha on Osteoblastic Differentiation of Isolated Synoviocytes and on Bone Explants from Arthritis Patients. Front Immunol. 2015;6:151.
51. Heftdal LD, Andersen T, Jaehger D, Woetmann A, Ostgard R, Kenngott EE, et al. Synovial cell production of IL-26 induces bone mineralization in spondyloarthritis. J Mol Med (Berl). 2017;95(7):779-87.
52. Cronstein BN, Aune TM. Methotrexate and its mechanisms of action in inflammatory arthritis. Nat Rev Rheumatol. 2020;16(3):145-54.
53. Gyori DS, Mocsai A. Osteoclast Signal Transduction During Bone Metastasis Formation. Front Cell Dev Biol. 2020;8:507.
54. Zhao Z, Hua Z, Luo X, Li Y, Yu L, Li M, et al. Application and pharmacological mechanism of methotrexate in rheumatoid arthritis. Biomed Pharmacother. 2022;150:113074.
55. Vanderplanck C, Ansseau E, Charron S, Stricwant N, Tassin A, Laoudj-Chenivesse D, et al. The FSHD atrophic myotube phenotype is caused by DUX4 expression. PLoS One. 2011;6(10):e26820.
56. Chang JH, Lee KJ, Kim SK, Yoo DH, Kang TY. Validity of SW982 synovial cell line for studying the drugs against rheumatoid arthritis in fluvastatin-induced apoptosis signaling model. Indian J Med Res. 2014;139(1):117-24.
57. Jones TI, Chen JC, Rahimov F, Homma S, Arashiro P, Beermann ML, et al. Facioscapulohumeral muscular dystrophy family studies of DUX4 expression: evidence for disease modifiers and a quantitative model of pathogenesis. Hum Mol Genet. 2012;21(20):4419-30.
58. Khansai M, Phitak T, Klangjorhor J, Udomrak S, Fanhchaksai K, Pothacharoen P, et al. Effects of sesamin on primary human synovial fibroblasts and SW982 cell line induced by tumor necrosis factor-alpha as a synovitis-like model. BMC Complement Altern Med. 2017;17(1):532.
59. Tassin A, Laoudj-Chenivesse D, Vanderplanck C, Barro M, Charron S, Ansseau E, et al. DUX4 expression in FSHD muscle cells: how could such a rare protein cause a myopathy? J Cell Mol Med. 2013;17(1):76-89.
60. Goossens K, Vandaele L, Wydooghe E, Thys M, Dewulf J, Peelman LJ, et al. The importance of adequate fixation for immunofluorescent staining of bovine embryos. Reprod Domest Anim. 2011;46(6):1098-103.
61. Hoetelmans RW, Prins FA, Cornelese-ten Velde I, van der Meer J, van de Velde CJ, van Dierendonck JH. Effects of acetone, methanol, or paraformaldehyde on cellular structure, visualized by reflection contrast microscopy and transmission and

scanning electron microscopy. Appl Immunohistochem Mol Morphol. 2001;9(4):346-51.
62. Choi SH, Gearhart MD, Cui Z, Bosnakovski D, Kim M, Schennum N, et al. DUX4 recruits p300/CBP through its C-terminus and induces global H3K27 acetylation changes. Nucleic Acids Res. 2016;44(11):5161-73.
63. Sasaki-Honda M, Jonouchi T, Arai M, Hotta A, Mitsuhashi S, Nishino I, et al. A patient-derived iPSC model revealed oxidative stress increases facioscapulohumeral muscular dystrophy-causative DUX4. Hum Mol Genet. 2018;27(23):4024-35.
64. Kowaljow V, Marcowycz A, Ansseau E, Conde CB, Sauvage S, Matteotti C, et al. The DUX4 gene at the FSHD1A locus encodes a pro-apoptotic protein. Neuromuscul Disord. 2007;17(8):611-23.
65. Yang B, Johnson TS, Thomas GL, Watson PF, Wagner B, Furness PN, et al. A shift in the Bax/Bcl-2 balance may activate caspase-3 and modulate apoptosis in experimental glomerulonephritis. Kidney Int. 2002;62(4):1301-13.
66. Porter AG, Janicke RU. Emerging roles of caspase-3 in apoptosis. Cell Death Differ. 1999;6(2):99-104.

Acknowledgements – I would like to thank Elien Luyten (E.L.) and Prof. dr. Pieter Ruytinx (P.R.) for all the guidance, life lessons, support, feedback, and their invaluable patience in the last 7 months. Furthermore, I also want to thank the Somers-Fraussen lab, especially Ellen Sleurs (E.S.), for the help and feedback on my lab work. Special thanks to Yanne Van Reusel and Elke Smeets for the help in scheduling the qPCRs and mental support. E.L. and P.R. designed the experiments. D.C., E.L., and E.S. performed RNA isolations, nested PCRs, PCRs, and qPCR. Transfection protocols were written by D.C. and carefully reviewed and executed by E.L. and P.R.. Antibody purification and peptide ELISA were performed by D.C.. Data analysis was performed by D.C. and E.L. under review of P.R.
Author contributions – D.C. wrote the thesis. All authors carefully reviewed the text.

SUPPLEMENTARY FIGURES AND TABLES

S1 - Overview of primers used in PCR, qPCR, and nested PCR

#	Gene	FW/RV	Length (bp)	Sequence (5' -- 3')	Modification	Manufact.	Ref. #	Used technique
1	*ZSCAN4*	FW	20	TGGAAATCAAGTGGCAAAAA		IDT	230287929	qPCR – DUX4 target genes
2	*ZSCAN4*	RV	18	CTGCATGTGGACGTGGAC		IDT	230287928	qPCR – DUX4 target genes
3	*MBD3L2*	FW	20	GCGTTCACCTCTTTTCCAAG		IDT	230287927	qPCR – DUX4 target genes
4	*MBD3L2*	RV	20	GCCATGTGGATTTCTCGTTT		IDT	230287926	qPCR – DUX4 target genes
5	*TRIM43*	FW	20	ACCCATCACTGGACTGGTGT		IDT	230287925	qPCR – DUX4 target genes
6	*TRIM43*	RV	20	CACATCCTCAAAGAGCCTGA		IDT	230287924	qPCR – DUX4 target genes
7	*PRAMEF1*	FW	20	GCTGGAACACCTTCAGTTGC		IDT	237937542	qPCR – DUX4 target genes
8	*PRAMEF1*	RV	20	AGTTCTCCAAGGGGTTCTGG		IDT	237937543	qPCR – DUX4 target genes
9	*DUX4*	FW	24	AGCTTTAGGACGCGGGGTTGGGAC		IDT	230287921	qPCR
10	*DUX4*	RV	20	GCAGGTCTGCWGGTACCTGG		IDT	230287920	qPCR
11	*GAPDH*	FW	22	GTCTCCTCTGACTTCAACAGCG		IDT	230287919	qPCR – House keeping gene
12	*GAPDH*	RV	22	ACCACCCTGTTGCTGTAGCCAA		IDT	230287918	qPCR – House keeping gene
13	*DUX4*	RV	19	CTTGCACGTCAGCCGGGGT		IDT	230905329	PCR
14	*DUX4*	FW	20	CGGAGAACTGCCTTTCTTTC		IDT	230905328	PCR
15	*DUX4*	RV	20	TCCAGGTTTGCCTAGACAGC		IDT	233167201	PCR, nested PCR* (ex 3)
16	*DUX4*	RV	20	ATGCCCAGGAAAGAAAGGCA		IDT	233167202	qPCR, PCR
17	*DUX4*	RV	20	CTCTCCAGATACCACGTTTC		IDT	233167204	nested PCR↓ (ex 7)
18	*DUX4*	RV	20	CTCACAAGGTCCTCTTACTG		IDT	233167205	nested PCR* (ex 7)
19	*DUX4*	FW	31	TACCTTAATTAA**G**atggccctcccgacaccc	PacI-**xtra G**	IDT	222603942	PCR
20	*DUX4*	FW	20	ctcagtgaggaagaataccg		IDT	238124410	qPCR, PCR, nested PCR↓ (ex 3 and 7)
21	*DUX4*	RV	20	ggtattcttcctcgctgagg		IDT	225761067	PCR
22	*DUX4*	FW	19	aggggcagatgcaaggcat		IDT	238124409	PCR, nested PCR* (ex 3 and 7)
23	*DUX4*	RV	20	aagaacaagggcacagagag		IDT	225761071	PCR, nested PCR↓ (ex 3)
24	*DUX4*	FW	28	TTAATCTAGA**A**atggccctcccgacacc		IDT	228786484	PCR

S1 continued – Overview of primers used in PCR, qPCR, and nested PCR

#	Gene	FW/RV	Length	Sequence (5' -- 3')	Modification	Manufact.	Ref. #	Used technique
25	*SOD1*	FW	20	GCACACTGGTGGTCCATGAA		IDT	235618008	qPCR – Stress genes
26	*SOD1*	RV	21	ACACCACAAGCCAAACGACTT		IDT	235618009	qPCR – Stress genes
27	*GPX1*	FW	25	GGTTTTCATCTATGAGGGTGTTTCC		IDT	235618014	qPCR – Stress genes
28	*GPX1*	RV	20	GCCTTGGTCTGGCAGAGACT		IDT	235618015	qPCR – Stress genes
29	*BAX*	FW	22	CCCTTTTCTACTTTGCCAGCAA		IDT	235618016	qPCR – Stress genes
30	*BAX*	RV	19	CCCGGAGGAAGTCCAATGT		IDT	235618017	qPCR – Stress genes
31	*BCL2*	FW	23	GAGGATTGTGGCCTTCTTTGAGT		IDT	235618018	qPCR – Stress genes
32	*BCL2*	RV	20	AGTCATCCACAGGGCGATGT		IDT	235618019	qPCR – Stress genes
33	*CASP3*	FW	22	TTTGAGCCTGAGCAGAGACATG		IDT	235618020	qPCR – Stress genes
34	*CASP3*	RV	22	TACCAGTGCGTATGGAGAAATGG		IDT	235618021	qPCR – Stress genes

** outer primer pair, ⸸: inner primer pair. ZSCAN4, Zinc Finger and Scan Domain Containing 4; MBD3L2, Methyl-CpG Binding Domain Protein 3 Like 2; TRIM43, Tripartite Motif Family 43; PRAMEF1, PRAME Family Member 1; DUX4, Double Homeobox 4; SOD1, Superoxide dismutase 1; GPX1, Glutathion peroxidase 1; BAX, BCL2 associated X protein; BCL2, B-cell lymphoma 2; CASP3, Caspase 3; GAPDH, Glyceraldehyde 3-phosphate dehydrogenase; IDT, Integrated DNA Technologies; PCR, Polymerase chain reaction; qPCR, quantitative PCR; ex, exon; FW, forward primer; RV, reverse primer; bp, base pair(s); A, adenine; C, cytosine; T, thymine; G, guanine; Manufact., manufacturer; Ref. #, reference number*.

S2 - Overview of antibodies used in immunofluorescent staining

Antibody	Target	Primary/Secondary	Manufact.	Ref. #
Mouse anti-human vimentin	Vimentin	Primary	Dako	M0725
Human anti-human DUX4	DUX4	Primary	Patient-isolated	IgG
Goat anti-mouse AF555	Mouse Fc	Secondary	Invitrogen	A21424
Goat anti-human AF555	Human Fc	Secondary	Invitrogen	A21433

Standard protocol - QuantStudio 3

Fast protocol - QuantStudio 3

S3 **- QuantStudio3 protocols**

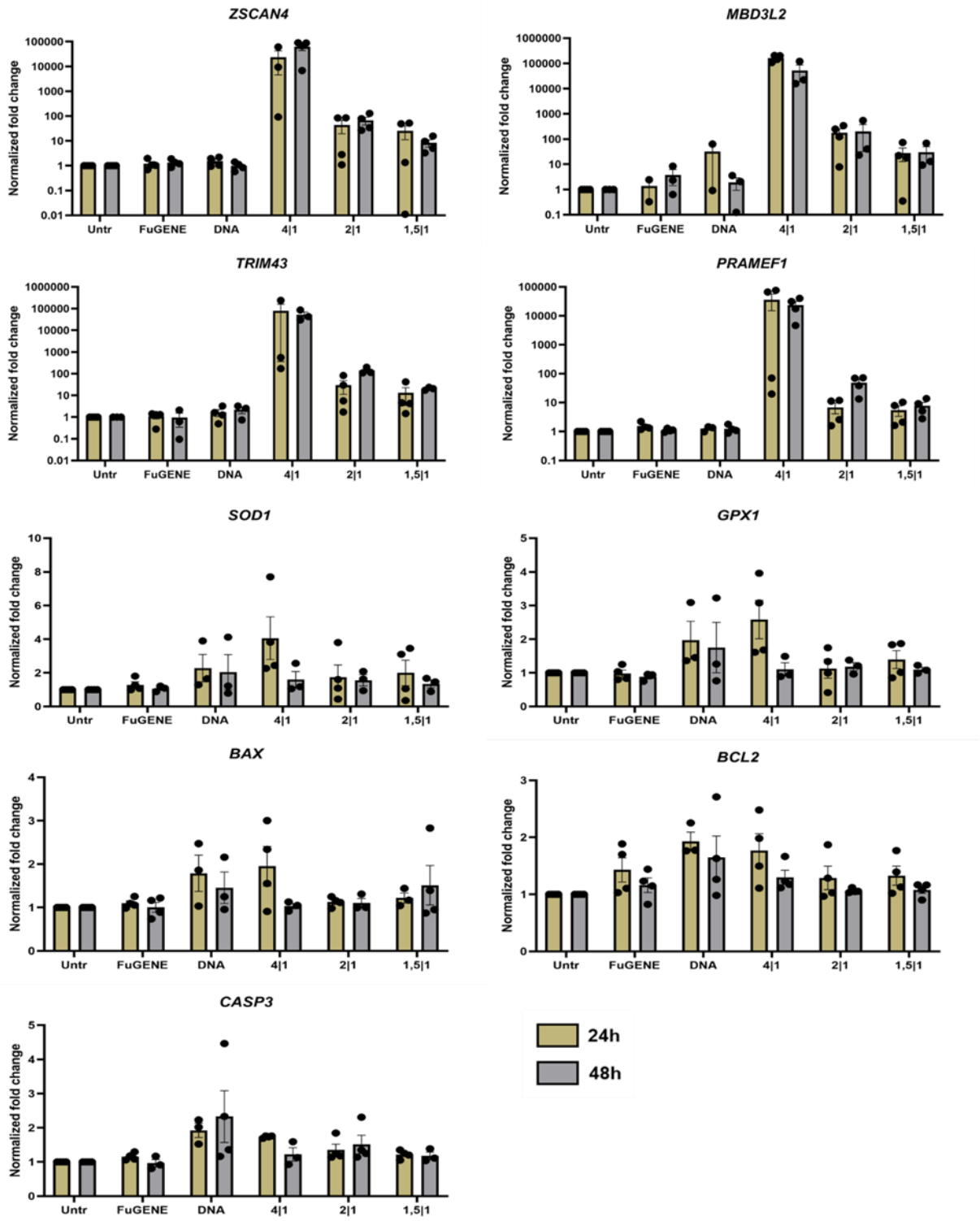

S4 - No significant differences in DUX4 target gene or stress gene expression were observed comparing 24 h and 48 h post-transfection with FuGENE. Fold changes were calculated using the 2-ΔΔCt method and normalized to the untransfected control (Untr). A549 cells were transfected with FuGENE in a 4:1 ratio of FuGENE reagent : plasmid (4|1), a 2:1 ratio (2|1) and a 1,5:1 ratio (1,5|1) for 24 h or 48 h. No significant differences in DUX4 target gene or stress gene expression were observed comparing 24 h (gold) to 48 h (silver). n = 3 – 4 for all genes except MBD3L2 which had n = 2 – 3. Time points were compared using a Mann-Whitney-U test and multiple comparisons Holm Sidak test at α= 0,05. *ZSCAN4, Zinc Finger and Scan Domain Containing 4; MBD3L2, Methyl-CpG Binding Domain Protein 3 Like 2; TRIM43, Tripartite Motif Family 43; PRAMEF1, PRAME Family Member 1; SOD1, Superoxide dismutase; GPX1, glutathione peroxidase 1; BAX, BCL2 associated X apoptosis regulator, BCL2, B-cell lymphoma 2; CASP3, Caspase 3.*

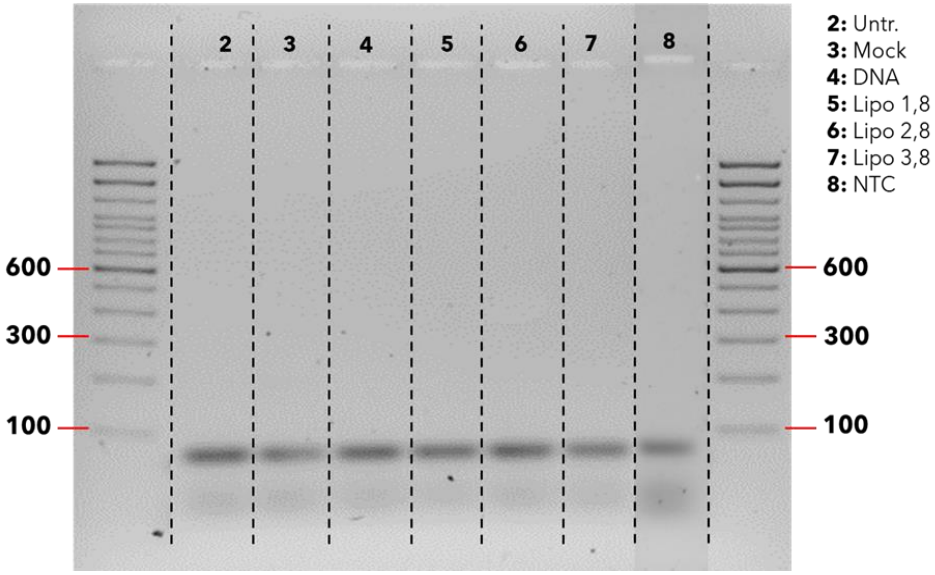

S5 – No DUX4 mRNA was detected in A549 cells by a regular 35-cycle PCR after 72 h transfection with Lipofectamine™3000. After 72h transfection of A549 with Lipofectamine™3000, no DUX4 mRNA was detected in any of the transfected conditions. A549 cells were transfected in different ratios of Lipofectamine™3000 to plasmid DNA: 1,8 : 1,8 (Lipo 1,8), 2,8 : 1,8 (Lipo 2,8) or 3,8 : 1,8 (Lipo 3,8). An untransfected (Untr), mock-transfected (Mock), and non-transfected (DNA) control were taken along and showed no DUX4 amplicon at the expected height of 604 bp. *bp, pase pair; NTC, no template control.*

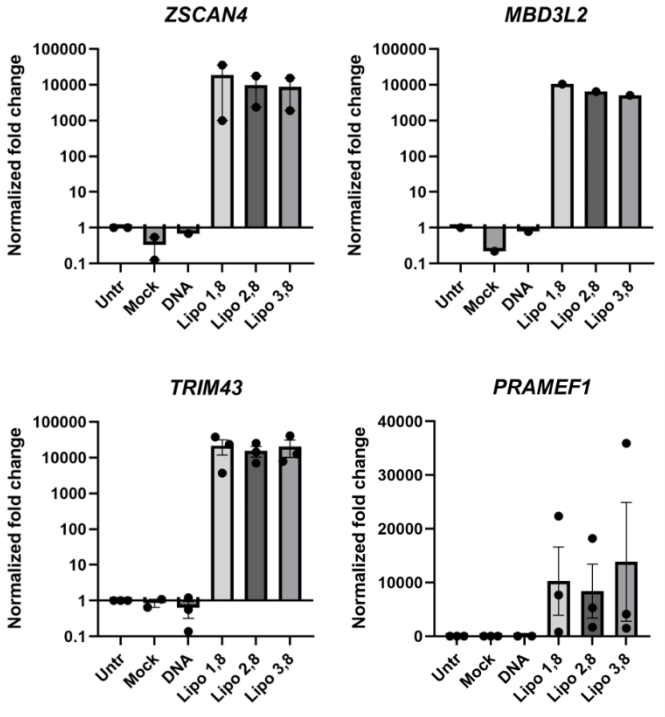

S6 - DUX4 target gene expression is increased upon 72h transfection with Lipofectamine™3000. Fold changes were calculated using the $2^{-\Delta\Delta Ct}$ method and normalized to the untransfected condition (Untr). A549 cells were transfected with Lipofectamine 3000 in a 3,8:1,8 ratio (Lipo 3,8), a 2,8:1,8 (Lipo 2,8), and a 1,8:1,8 (Lipo 1,8) ratio. DUX4 target gene increased in alle three transfected condition to a comparable level. The Mock and DNA control conditions had gene expression level similar to the untransfected control. *n = 2 for ZSCAN4, n = 1 for MBD3L2, n = 2 - 3 for TRIM43 and n = 3 for PRAMEF1. Statistical significance was assessed for TRIM43 and PRAMEF1 using a Kruskal-Wallis test. ZSCAN4, Zinc Finger and Scan Domain Containing 4; MBD3L2, Methyl-CpG Binding Domain protein 3 Like 2; TRIM43; Tripartite Motif Family 43; PRAMEF1, PRAME Family Member 1.*

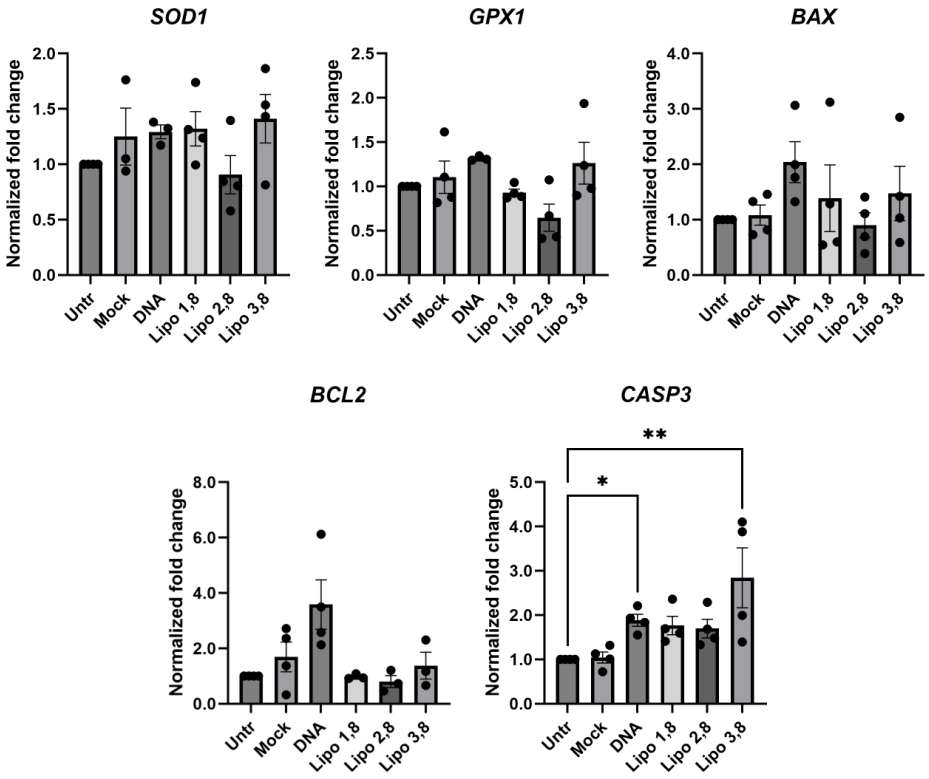

S7 – 72 h transfection with Lipofectamine™3000 in a 3,8:1,8 ratio increased *CASP3* mRNA levels significantly. Fold changes were calculated using the $2^{-\Delta\Delta Ct}$ method and normalized to the untransfected control (Untr). Transfection of A549 cells with Lipofectamine™3000 or 72 h did not alter gene expression of *SOD1*, *GPX1*, *BAX*, or *BCL2*. However, *CASP3* gene expression was significantly increased upon transfection in a 3,8:1,8 ratio. *n = 3 – 4, statistical significance was assessed using a Kruskal-Wallis test and a post-hoc Dunn's test comparing each group to the untransfected control (Untr). * p < 0,05, ** p < 0,01. SOD1, Superoxide dismutase; GPX1, glutathione peroxidase 1; BAX, BCL2 associated X apoptosis regulator, BCL2, B-cell lymphoma 2; CASP3, Caspase 3.*

Supplementary methods

Purification of UH-axSpA-IgG.8 from patient plasma

UH-axSpA-IgG.8 antibodies were purified from plasma samples of arthritis patients using streptavidin biotin-based affinity chromatography. In brief, Pierce™ spin columns (cat. No. 69705, Thermo Scientific, United States) were packed with 50 µL of high-capacity streptavidin agarose resin (slurry, cat. No. 20357, Thermo Scientific, United States), centrifugated at 500 g for 1' and washed with 1X PBS to resuspend the resin and to equilibrate the column. Then, the column was washed thrice by adding 1X PBS and centrifugation for 1' at 500 g.

Next, biotinylated peptide 8 (0,5 mg/mL, GL Biochem) was diluted 1:2 in 2X PBS, and 50 µg of peptide was loaded for coupling onto the column and incubated on a rotating mixer (90 rpm) at RT for 1 h. The column was then centrifugated again, and the flowthrough was stored at 4°C. Following peptide coupling, the column was washed again three times. Then, the plasma sample was diluted 9:1 with 10X PBS, loaded onto the column, and incubated for 2 h on a rotating mixer at 4°C. After centrifugation, the flowthrough was stored at 4°C. Ultimately, the column was eluted four times. into Eppendorfs containing 7 µL neutralization buffer (1M Tris-HCl, pH 9). Here, 125 µL elution buffer (100 mM glycine, pH 2,5) was added to the column, incubated for 2' at room temperature, and centrifuged for 1' at 500 g. The yield of each sample was determined using Nanodrop™ 2000. The first and second elution fractions were aliquoted and dialyzed to 1X PBS overnight at 4°C.

Peptide Enzyme-Linked ImmunoSorbent Assay

To assess the immunoreactivity of the purified UH-axSpA-IgG.8 antibodies, a peptide ELISA was executed. A 96 half-well plate (ref 675061 Greiner Bio-One, Austria) was coated with peptide 8 (0,5 mg/mL, Biomatik, Canada) or control peptide (2,0 mg/mL, Biomatik, Canada) at a coating concentration of 2 µg/mL in 1X PBS and set overnight at 4°C.

The next day, the plate was washed using 0,5% Tween 20 (cat. no 8.22184.0500, VWR, United States) in 1X PBS. Wells were blocked with 2% Marvel in 1X PBS (PBS-M) for 2 h at 37°C and 90 rpm on an orbital shaker. Wells were washed again, and a standard curve for peptide 8 and control peptide was implemented by diluting a positive healthy control standard for each in PBS-M. Samples were diluted 1:50 and/or 1:100 in PBS-M. Then, 50 µL/well of diluted samples were added to the wells and incubated for 2 h at 90 rpm at RT. Next, the secondary antibody, HRP-labeled polyclonal rabbit anti-human IgG (Dako, P0214), was diluted 1:2000, added to the wells, and incubated for 1 h at RT and 90 rpm.

Next, 3,3',5,5'-tetramethylbenzidine (TMB, ref. 34029, Thermo Scientific, United States) was added to the wells and kept in the dark for 10' to allow the blue reaction product to be formed. Lastly, the enzymatic reaction was stopped using 1,8 N sulfuric acid, and the absorbance was measured at 450 nm using the CLARIOstar® Plus (BMG Labtech, Germany).